AD-A171 528 DUST PARTICLE VELOCITY MEASUREMENT IN SHOCK TUBES(U) 1/1
SPECTRON DEVELOPMENT LABS INC COSTA MESA CA
D MODARRESS 08 DEC 85 SDL-86-2368-22 DNA-TR-86-12
UNCLASSIFIED DNA001-84-C-0116 F/G 14/2 NN

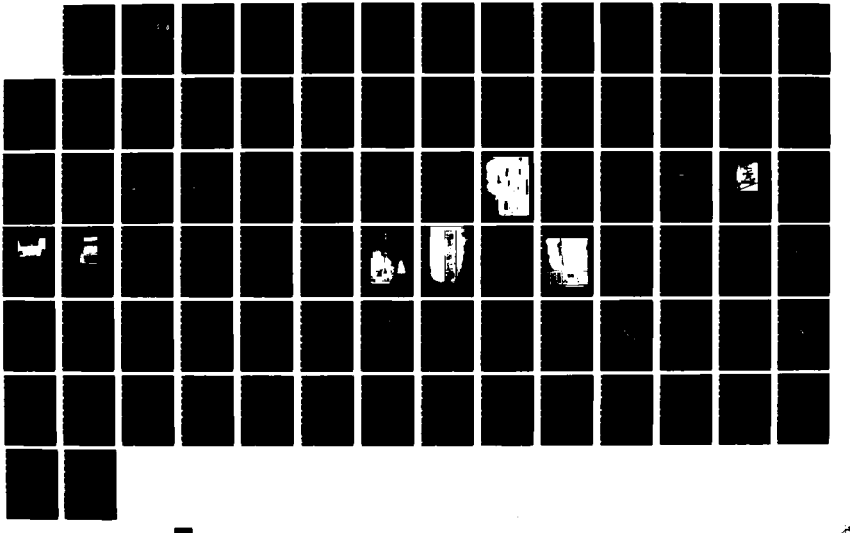

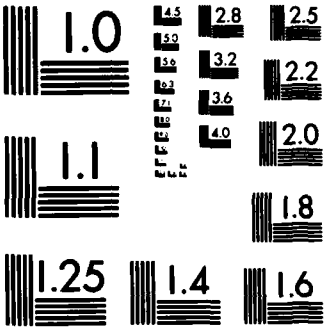

(12)

AD-A171 528

DNA-TR-86-12

DUST PARTICLE VELOCITY MEASUREMENT IN SHOCK TUBES

Dariush Modarress
Spectron Development Laboratories, Inc.
3303 Harbor Blvd.
Costa Mesa, CA 92626-1579

8 December 1985

Technical Report

CONTRACT No. DNA 001-84-C-0116

Approved for public release;
distribution is unlimited.

THIS WORK WAS SPONSORED BY THE DEFENSE NUCLEAR AGENCY
UNDER RDT&E RMSS CODE X341084469 Q93QMXAG00004 H2590D.

Prepared for
Director
DEFENSE NUCLEAR AGENCY
Washington, DC 20305-1000

DISTRIBUTION LIST UPDATE

This mailer is provided to enable DNA to maintain current distribution lists for reports. We would appreciate your providing the requested information.

☐ Add the individual listed to your distribution list.

☐ Delete the cited organization/individual

☐ Change of address.

NAME: _____

ORGANIZATION: _____

OLD ADDRESS	CURRENT ADDRESS
_____	_____
_____	_____
_____	_____

TELEPHONE NUMBER: ( ) _____

SUBJECT AREA(s) OF INTEREST:

_____	_____
_____	_____
_____	_____

DNA OR OTHER GOVERNMENT CONTRACT NUMBER: _____

CERTIFICATION OF NEED-TO-KNOW BY GOVERNMENT SPONSOR (if other than DNA):

SPONSORING ORGANIZATION: _____

CONTRACTING OFFICER OR REPRESENTATIVE: _____

SIGNATURE: _____

UNCLASSIFIED
SECURITY CLASSIFICATION OF THIS PAGE

AD-A171528

REPORT DOCUMENTATION PAGE

Form Approved
OMB No. 0704-0188
Exp. Date: Jun 30, 1986

1a. REPORT SECURITY CLASSIFICATION UNCLASSIFIED	1b. RESTRICTIVE MARKINGS
2a. SECURITY CLASSIFICATION AUTHORITY N/A since Unclassified	3. DISTRIBUTION/AVAILABILITY OF REPORT Approved for public release; distribution is unlimited.
2b. DECLASSIFICATION/DOWNGRADING SCHEDULE N/A since Unclassified	
4. PERFORMING ORGANIZATION REPORT NUMBER(S) 86-2368-22	5. MONITORING ORGANIZATION REPORT NUMBER(S) DNA-TR-86-12
6a. NAME OF PERFORMING ORGANIZATION Spectron Development Laboratories, Inc. 6b. OFFICE SYMBOL (If applicable)	7a. NAME OF MONITORING ORGANIZATION Director Defense Nuclear Agency
6c. ADDRESS (City, State, and ZIP Code) 3303 Harbor Blvd. Costa Mesa, CA 92626-1579	7b. ADDRESS (City, State, and ZIP Code) Washington, DC 20305-1000
8a. NAME OF FUNDING/SPONSORING ORGANIZATION 8b. OFFICE SYMBOL (If applicable)	9. PROCUREMENT INSTRUMENT IDENTIFICATION NUMBER DNA 001-84-C-0116
8c. ADDRESS (City, State, and ZIP Code)	10. SOURCE OF FUNDING NUMBERS

PROGRAM ELEMENT NO	PROJECT NO	TASK NO	WORK UNIT ACCESSION NO.
62715H	Q93QMXA	G	DH251119

11. TITLE (Include Security Classification)
DUST PARTICLE VELOCITY MEASUREMENT IN SHOCK TUBES

12. PERSONAL AUTHOR(S)
Modarress, Dariush

13a. TYPE OF REPORT	13b. TIME COVERED	14. DATE OF REPORT (Year, Month, Day)	15. PAGE COUNT
Technical	FROM 840201 TO 850930	851208	82

16. SUPPLEMENTARY NOTATION
This work was sponsored by the Defense Nuclear Agency under RDT&E RMSS Code X341084469 Q93QMXAG00004 H2590D.

17 COSATI CODES			18. SUBJECT TERMS (Continue on reverse if necessary and identify by block number)
FIELD	GROUP	SUB-GROUP	
14	2		Velocity, Shock Tube, Dusty, Boundary Layer
20	11		

19. ABSTRACT (Continue on reverse if necessary and identify by block number)

The results of particle velocity measurements at TRW's 4 x 4 inch shock tube and at the CERF 6' shock tube are presented. At both sites, measurements were made in a dusty boundary layer induced by a shock wave passing over a dusty bed. The dust particle velocity was measured using a single component laser velocimeter at CERF. At both sites, the transient data was recorded using a 100 MHz digitizer. Processing of the data was done through software. The velocity time history of the dust particles behind the moving shock waves was measured at various heights.

20. DISTRIBUTION/AVAILABILITY OF ABSTRACT	21. ABSTRACT SECURITY CLASSIFICATION
☐ UNCLASSIFIED/UNLIMITED ☒ SAME AS RPT ☐ DTIC USERS	UNCLASSIFIED

22a. NAME OF RESPONSIBLE INDIVIDUAL	22b. TELEPHONE (Include Area Code)	22c. OFFICE SYMBOL
Betty L. Fox	(202) 325-7042	DNA/STTI

DD FORM 1473, 84 MAR — 83 APR edition may be used until exhausted. All other editions are obsolete.

SECURITY CLASSIFICATION OF THIS PAGE
UNCLASSIFIED

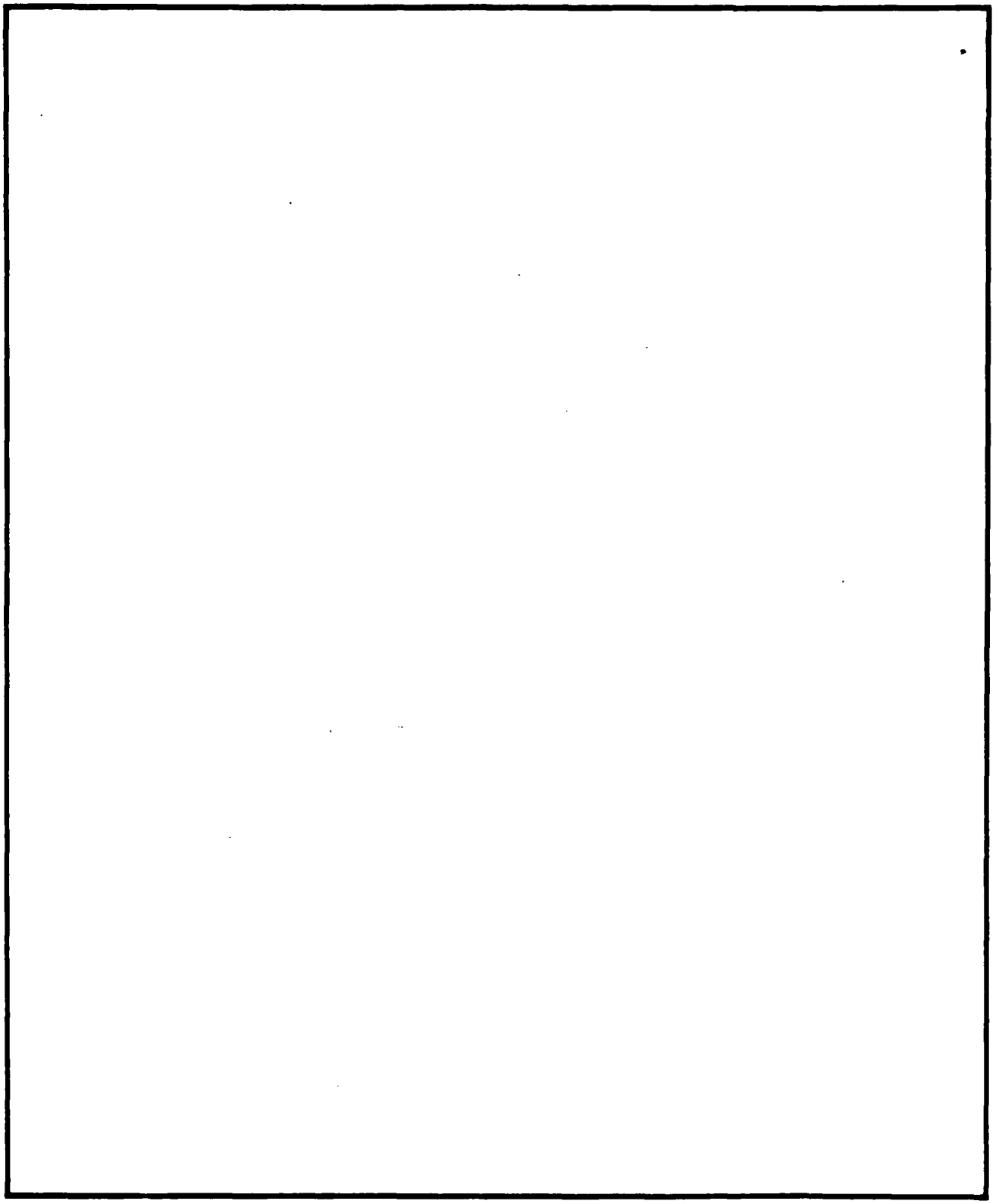

SUMMARY

The results obtained during first phase of a program for measurement of dust particle velocity in shock tubes are presented. A detailed description of laser velocimetry instrumentation designed for the measurement at TRW 4 X 4 inch and CERF 6' shock tubes are presented. Limited number of measurement data were obtained in both shock tubes. Data for streamwise velocity, normal velocity and dust density for some portion of the flow where optical measurement is achievable is presented. The results clearly show the development of dust boundary layer behind the moving shock wave. The boundary layer height defined by the presence of dust particles was found to be larger than those defined by the gradient of the steam wise velocity. Through simultaneous measurement of laser light extinction and particle classification for a portion of measurement period, it was possible to estimate the dust density profile at the TRW 4 x 4" shock tube.

CONVERSION TABLE

Conversion factors for U.S. Customary

to metric (SI) units of measurements

MULTIPLY → / ← TO GET	BY → / ← BY	TO GET → / ← DIVIDE
atmosphere (normal)	1.013 25 X E +2	kilo pascal (kPa)
bar	1.000 000 X E +2	kilo pascal (kPa)
degree (angle)	1.745 329 X E -2	radian (rad)
foot	3.048 000 X E -1	meter (m)
inch	2.540 000 X E -2	meter (m)
micron (μ)	1.000 000 X E -6	meter (m)
pound-force (lbs) avoirdupois	4.448 222	newton (N)
pound-force inch	1.129 848 X E -1	newton-meter (N.m)
pound-force/foot^2	4.788 026 X E -2	kilo pascal (kPa)
pound-force/inch^2 (psi)	6.894 757	kilo pascal (kPa)
pound-mass (lbm avoirdupois)	4.535 924 X E -1	kilogram (kg)
pound-mass/foot^3	1.601 846 X E +1	kilogram/meter^3 (kg/m^3)

TABLE OF CONTENTS

LIST OF ILLUSTRATIONS

LIST OF ILLUSTRATIONS (CONTINUED)

LIST OF ILLUSTRATIONS (CONCLUDED)

SECTION 1
INTRODUCTION

Parameters of interest associated with the passage of shock wave over a dust bed include the mass lofting rate, dust velocity profile, and dust mass loading profile. The data on these and similar topics should help in the understanding of the complicated interaction between the gas and the solid phase of the flow. This interaction becomes even more complicated in the presence of a high sound speed region.

To fully justify the measurement requirements, a comprehensive parametric experimental study of the flows was required. This study was beyond the scope of the reporting program. However, in this report, the diagnostic instrumentation required for the velocity and dust density measurement are described and the results of the initial measurements are reported.

1.1 PREDICTION OF PARTICLE TRAJECTORY.

The calculation presented here was performed solely to obtain a rough estimate of the particle dynamics in order to guide the design of the experiment and to help analyze the measured data. To determine the measurement location of the multipoint velocimeters, a simple numerical evaluation of the particle trajectory was made by solving the equations of motion for an isolated particle. The primary force on the particle was assumed to be that of drag, a function of the particle Reynolds Number. The gravitational force was also included in the equation of motion in the vertical direction. The gas velocity profile was assumed to be known and taken from the measurement of Reference 1. Here, data was available for an overpressure of 23 psi (158.6 k Pa). Initial trajectory of the particle into the boundary layer was taken from the same reference.

The particle trajectory calculation was first carried out for a 2 mm diameter particle for which the data were available (ref. 1). The results are given in Figure 1. It shows good agreement between the experiment and the computed results.

Similar calculations for overpressures of 205 and 410 k Pa were carried out. In the absence of better models, the gas velocity profiles were assumed to scale with those measured for the overpressure of 23 psi (168 k Pa). The initial particle trajectory angle of 40 Degrees, and initial particle velocity equal to 2% of the freestream gas velocity were assumed. The results are shown in Figures 2 and 3. Figure 2 shows the trajectory of the particles during the initial phase of the lift off. The smaller particles lose their initial momentum rapidly and follow the gas stream. The larger particles, due to their larger initial momentum, penetrate the gas boundary layer. The results show the classic mechanism of aerodynamic sorting of the particles.

It should be pointed out that the smaller particles are more influenced by the turbulence within the boundary layer (not modeled here), and hence are apt to be more uniformly dispersed within the flow field. Hence, a uniform sorting of the particles according to their size, as predicted here, should not be expected. On the other hand, the larger particles are less affected by the velocity fluctuations so their distributions are probably more accurately presented here.

Figure 3 shows the trajectories of different particles and their expected elevation as a function of time. The position of the measurement stations are also included. Based on this model, the length of the dust bed must be at least 17 meters so as to expect a 100 micron particle to reach a height of 20 centimeters, our highest measurement locations at CERF 6' shock tube. These numbers were used as a guideline for the CERF 6' shock tube measurements.

An estimate of the particle relaxation time for two overpressures of 205 and 410 psi were made and shown in Figure 4. It shows that first, the overpressure does not greatly influence the relaxation period of the particles, and secondly, a relaxation time of the order of 10 ms (for predicted velocity jump across the shock wave) is predicted for 100 micron particles. This information, used as an order of magnitiude information, helps determine the minimum measurement time required for any given particle size to reach equilibrium within the carrying flow.

SECTION 2
INSTRUMENTATION

The components of the experimental subject matter are briefly described herein. These include, the principle of operation for the measurement technique, and the description of the apparatus designed for the measurments. In each case, the shock tube used in the experiment is briefly described, and then the apparatus designed for the measurement is reviewed.

2.1 PRINCIPLE OF OPERATION.

Direct measurement of the particle velocity was obtained using Laser Doppler Velocimetry (LDV) [Ref. 2 and 3]. The apparatus generally consists of a coherent source of light (laser) included in a transmitting optics, and receiving optics as depicted in Figure 5. Two coherent beams are focused at the measurement point, known as the probe volume, resulting in the formation of the interference fringes. The distance between fringes (δ) is determined by the beam angle (θ) and the laser beam wavelength (λ) as given by

$$\theta = \lambda/2 \sin(\theta/2) \tag{1}$$

When a particle with a velocity U crosses the probe volume, it scatters light proportional to the local intensity of the light. The receiving optics collects portion of the light and transforms it into an electrical signal, known as Doppler burst. The period of the burst (τ) is a function of the fringe spacing and the instantaneous velocity of the particle, U. Through direct digitization of the signal and post processing, the particle velocity may be obtained from the relation

$$U = (\delta/\tau) \tag{2}$$

Simultaneous measurement of the opacity of the measurement media is made with the use of a photodiode as a beam stop. The reduction of the total

optical energy collected on the photodiode can theoretically be related to the increase in the dust loading in the shock tube test section. Here, assumptions are made that the scattering characteristics of the dust particles are uniform; that the amount of light scattered is proportional to the scattering cross section of the particles; and that the effect of the window contaminations are negligible.

2.2 TRW 4 X 4 INCH SHOCK TUBE.

A schematic of the shock tube at TRW is shown in Figure 6. It has a cross section of 3.5 by 3.5 inches (8.9 by 8.9 cm) with the floor replaced by a dust bed nominally 15 cm inches deep. The dust particle size range was 1 to 400 microns, with a mass mean of 120 microns. The shock tube configuration characteristics are summarized in Table 1. Optical access to the flow field was made through two 15 cm diameter windows. The test duration was 5 ms, limited by the dust bed leading characteristic [Ref. 4, 5]. The shock overpressure at the test section was nominally at 210 k Pa.

Laser Velocimeter. Measurement of the dust particle velocity was made using a single component, fringe mode, Laser Doppler Velocimeter as shown in Figure 7. A 4-watt Argon Ion laser operating in single frequncy mode was used. The light beam was focused onto a bragg cell used both as a beamsplitter and for frequency shifting. The beams were further collimated through a second lens, and crossed over at the probe volume by the transmitting lens. The scattered light was collected in back scatter mode onto the end of a fiber optic cable which carried the collected scattered light to a suitable photomultiplier. A photograph of the optical system, including the shock tube is shown in Figure 8.

An important criteria to the success of the measurement was to maximize the number of samples collected during each time window. Since the number of scattering centers could not be increased, as they were provided by the dust bed, the data collection was designed to maximize

Table 1. TRW 4" Shock Tube Conditions.

Nominal Test Overpressure	210 k Pa
Nominal Test Time	5 ms
Test Section Dimension	8.9 cm x 8.9 cm
Test Section Length	1.57 m
Dust Bed Material 40-48% Porosity	White Sands Natural
Specific Gravity 1-5 (noncompacted) 1-74 (compacted)	2-9 (solid only)
Particle Size average ~ 120 μm	d < 420 μm, mass mean

the acceptance rate of Doppler bursts. The pedestal of the amplified signal was first removed through a high pass filter. The signal was then mixed down with a 30 MHz signal to enable the signal to be digitized at a rate of 100 MHz. With the available total memory of 512K a real time recording duration of 5.12 ms was achieved. The recorded data were transferred to recording disks for archiving and retrieval. The block diagram of the data acquisition system is shown in Figure 9.

2.3 CERF 6' SHOCK TUBE.

The 6' Shock Tube located at Civil Engineering Research Facility (CERF) is made of 6' (1.97 m) diameter steel sections shown in Figure 10. The velocity measurements were made at Section G, 71 m from the opening in the driver side and approximatly 23 m into the dusty section.

The instrumentation was inside a concrete bunker placed underneath the shock tube as shown in Figure 11. The optical probe was placed over a traversing mechanism, Figure 12, and raised into the shock tube through an opening at the bottom of the tube. The probe inside the

shock tube was protected by a blast wing shown in Figures 13 and 14. The window plate was designed such that the measurement height, defined by the position of the optical probe, could be continuously varied. Figure 15 shows the photograph of the concrete bunker used in this experiment. The shock tube configuration is given in Table 2.

Table 2. Cerf 6' Shock Tube Conditions.

Nominal Test Overpressure	210 k Pa
Nominal Test Time	5 ms
Test Section Length	29.5 m
Test Bed Material	McCormick Ranch Natural
Particle Size mean 100 μ	d < 5000 μ

2.3.1 Multipoint Laser Velocimeter.

A four-point simultaneous velocimeter was designed for this test using a 4-watt Argon Ion laser. Again, a bragg cell was employed as a beamsplitter and for frequency shift, as shown in Figure 16. The two coherent beams of equal intensity were divided into four separate LDV's, through a series of beamsplitters. Approximately 25% of the laser power was directed to each station. The transmitting optics consisted of turning mirrors and focusing lenses. The receiving optics were also placed on the same support beam as the transmitting optics, and focused the scattered light onto four fiber optics cables. The details of the optical head assembly is shown in Figure 17. The optical probe and a close up of the optical head assembly are shown in Figures 18 and 19.

2.3.2 Data Acquisition.

The system diagram for the four component laser velocimeter is shown in Figure 20. The four fiber cables transmit the collected light to Photomultiplier Tubes. The signals are then amplified and run

through a multiplexer which transmits one signal according to a preprogramed schedule. This multiplexing is done in order to conserve the digital memory. The output of the multiplexer is then mixed down and recorded using a 100 MHz transient recorder. The entire data acquisition and trigger and firing sequence is controlled by an IBM PC. A photograph of the electronic instrumentation is shown in Figure 21.

2.3.3 Data Analysis.

An important aspect of the data acquisition of a laser velocimeter system is the method by which the signal is processed. Here, the velocity information (signal) should be separated from the anomalies (noise) in some form or fashion. In the present system, since the unedited data were recorded, various analysis algorithms were applied to an identical set of data and the relative effectiveness of the techniques were evaluated. Two of the major techniques which were implemented are briefly discussed here.

2.3.4 Three Level Comparator and a Phase Noise Detector.

A software version of the "three level comparator technique" was implemented. This technique has been successfully used in commercially available analogue counters. Here, positive and negative voltage thresholds are chosen. Each filtered burst is evaluated by the sequence at which the signal crosses the two thresholds and the zero voltage line. Here, the criteria is that at least one digitized point lies between two successive zero crossing points. In practice, the threshold values are chosen to be above the background noise, and yet to be smaller than the signal voltages. The effectiveness of the technique depends on the choice of the threshold. In our case, as we had access to the actual signal which is going to be processed, the level of the background noise during each time window was evaluated and the values of the threshold were automatically optimized. Figure 22 shows a typical burst processed using this technique.

A criteria for detection of phase noise in the signal was developed. Phase noise usually is generated when more than one particle is present at the probe volume. Here, the time rate of change of the signal was used as the test vehicle. In the absence of phase noise, the first derivative of the signal between any two successive zero crossing changes sign no more than two times. A signal with more than two changes of the sign of its derivative between successive zero crossings was then rejected.

An additional criteria comparing the calculated period of two different numbers of cycles of the same burst was also included in the discrimination software. This provided an additional test for the accuracy of the discriminating technique. Through the software, the effects of each discriminating technique were evaluated. It was determined that the combination of the above mentioned techniques, with as few as three full cycles of the burst, was sufficient for processing the signal obtained in the shock tube.

2.3.5 Burst Correlation/Frequency Spectrum Technique.

Another technique which was found to be more powerful for the cases of low signal-to-noise ratios and limited sample is described here. The particle velocity is assumed to be constant in every time window of 128 microseconds. Within each time window, bursts are recognized by a voltage threshold test. The acceptable bursts are recognized through their respective power spectra. Fast Fourier Transformation is used and the signal power distribution in the frequency domain is obtained. A criteria is used here to distinguish between acceptable and unacceptable signals. The acceptable bursts are further smoothed through autocorrelation. Finally, the mean velocity and standard deviation are obtained by Fourier Transformation of the mean autocorrelation of the bursts during of time window. Figure 23 shows a typical burst processed using spectrum analysis.

Figure 24 exhibits three typical "bursts" reproduced from the shock tube data set. They represent a strong signal, a marginal signal,

and what appears to be a very weak signal or possibly a random noise. When a "three level comparator" discrimination is applied to the above traces, only the first trace is accepted and the remainder are rejected. On the other hand, when the power spectrum of the signals are calculated, as shown in Figure 24, the frequency content and the strength of the signal for each burst is evaluated. In this case, the dominant frequency in all three bursts are close to each other, while the signal strength is different.

SECTION 3
MEASUREMENT MATRIX

Limited number of shock tube entries were made during the course of the present contract. The measurements were conducted in dusty non-precursed flows. The run conditions for the two shock tubes were generally different and no attempt is made here to correlate data beyond the overall features of the dusty boundary layer flows. More comprehensive investigation of the flows is curently being carried out using the instrumentation described in this report through our present contract (DNA001-84-C-0116) with the Defense Nuclear Agency (DNA).

3.1 TRW 4 X 4 INCH SHOCK TUBE.

Measurements were obtained at a test section located 3.6 m from the leading edge of the dust bed. The laser velocimeter was placed on an isolation table. The height of the probe volume was adjusted through elevation of the entire table. The shock tube operated by pressurizing the driver until bursting an aluminum diaphragm. The general flow parameters of the flow field are given in Table 1. The dust bed preparation consisted of running the tube a few times to achieve complete compactness of the dust bed. The surface of the dust bed was smoothed prior to each shot. The flow conditions were generally kept uniform for subsequent shots.

The shock tube driver was operated for a nominal 210 k Pa overpressure at the test section (with no dust). The strength of the shockwave however, was reduced as it passed over the dust bed. The pressure time history at the measurement location is shown in Figure 25. It shows a square wave profile for a duration of approximately 5 ms. The limiting wave was the compression from the leading edge of the soil bed. The peak over pressure was measured to be roughly 138 k Pa.

3.2 CERF 6' SHOCK TUBE.

Measurements were obtained at a test section located 70 meters from the start of the dust bed. The height of the probe was varied using the traversing mechanism (Figure 12). The general flow parameters are given in Table 2. The dust bed was compacted by a roller before each shot, and the driver was kept in the same configuration with the same charge level to maintain the same flow conditions for each shot.

The shock tube driver produced a nominal overpressure of 210 k Pa at the measurement position. The time history at this position is shown in Figure 26. It shows that the pressure declines approximately 35 k Pa for the 5 ms duration.

SECTION 4
RESULTS

Presentation of the results of the measurement are made in this chapter. The data are grouped in three categories:

1. Dust velocity data at TRW 4" shock tube.
2. Dust concentration data at TRW 4" shock tube.
3. Dust velocity data at CERF 6' shock tube.

In each case, the data acquisition was initiated by the passage of the shock wave at the measurement point and stopped after the memory bank was filled. No data compression was attempted. With 512k bytes of memory available, the total measurement duration in each case was limited to about 5 ms, coinciding roughly with the run duration of the shock tubes.

4.1 DUST VELOCITY DATA AT TRW 4" SHOCK TUBE.

During each run of the shock tube, only one component of the particle velocity was obtained. The dust surface preparation and the driver conditions were repeated for subsequent runs. The shock tube conditions and the static overpressure profiles are given in Table 1.

Figures 27 to 30 give the velocity data for the measurement heights of 6 mm (0.25 inch) to 25.4 mm (1 inch) above the initial dust level. In each case, the data obtained at the same height for different runs are presented together. The velocity data at 6 mm (.25 inch) is shown in Figure 27. The first arrival of particles at the measurement location was about .25 ms after the passage of the shock wave. This arrival time was consistent for all runs. During the subsequent 1.5 ms, an increase in the particle velocity is observed. This represents the response of the particles to the step function in the gas velocity behind the moving shock wave.

The vertical component of the dust particle velocity at the same measurement height is also given in Figure 28. Measurement consistency of the runs presented are very good. The normal velocity component shows a slow change in the angularity of the flow of the dust particles. At 1.5 ms after passage of the shock, the flow angle is measured to be about 10 degrees. This angle indicates the development of a boundary layer near the dust surface.

The development of the boundary layer is more apparent from the velocity data recorded at the height of 6 mm (same as Figure 27), but recorded for 4 ms as presented in Figure 31. The dust velocity shows a gradual decline after 1.5 ms, representing the growth of the boundary layer beyond the measurement height.

Similar data are obtained at heights of 13 mm (.5inch), 19 mm (.75inch), and 25 mm (1.0 inch), and are shown in Figures 28 to 30. The overall behavior of the dust particles are similar. This similarity is further demonstrated in Figure 32, where all the measurements are drawn together. It clearly shows the initial particle relaxation period of approximately 2 ms. The early time ($t < 1$ ms) velocity development behind the shockwave show a plug flow type of velocity field. The scatter of the data in this region may be attributed to the variation in the particle size distribution, as well as variation in the shock tube condition. The development of the velocity gradient (and hence, the velocity boundary layer) is also apparent. Based on the data of Figure 32, it is estimated that the velocity boundary layer reaches the highest measurement height of 25 mm (1 inch) at about 4 ms.

From the velocity time histories of proceeding figures, two boundary layer type profiles may be defined. One is determined by the arrival time of the dust particle at each of the measurement heights as shown in Figure 33. The second profile, also shown in the same figure, is defined by the points in Figure 32, for which the time rate of change of velocity becomes negative. This suggests that in dusty flows, the customery definition of the boundary layer must be augmented to distinguish between it and the boundary layer defined by the presence of the dust particles.

An important piece of data used for the evaluation of the computation prediction of the dusty flow is the velocity profile. Here, the velocity profile obtained at 4 ms behind the shock wave is plotted in Figure 34. The height of the "velocity" boundary layer was assumed to be 25 mm (1 inch). It was apparent that four points were not sufficient to clearly define the velocity profile. But it was also recognized that within the constraints of the measurement environment and the uncertainty of the dust bed, measurement closer to the surface was not possible. Figure 34 also shows the velocity data to best fit a 1/4 or 1/5 power law profile.

4.2 DUST CONCENTRATION DATA AT TRW 4" SHOCK TUBE.

As shown in Figure 5 of Section 2, a photodiode was used as the laser light beam stop when measurement at TRW 4" shock tube was made. The output of the photodiode registered the total laser power transmitted through the shock tube test section. Figures 35 to 38 show the raw data obtained at the measurement heights. The reduction in the transmitted laser power after the passage of the shock wave is caused by the presence of the scattering centers (dust particles) along the path of the beams in the shock tube. This response includes the buildup of the dust on the window which at its highest is estimated to scatter about 20% of the incident laser power. It was, however, decided that due to the uncertainty of the rate of the dust buildup on the window during the first few milliseconds, no correction will be applied to the measured data. The combined plots of the extinction curves are given in Figure 39.

Data on the particle size distribution at the measurement location is required to reduce the laser light extinction to dust concentration data. This information was, however, not available for all time as independent measurement of the particle size was not measured. (This measurement is presently being carried out at the TRW 17" shock tube). There were, however, regions in the early measurement time history where it was determined that the particle size distribution

to be roughly between 1 and 10 micrometers. This time region was bounded by the onset of the laser extinction light, and the arrival of the larger than 10 micron particles determined from the velocity measurements and shown in Figure 40. Based on the uniform weight distribution (cube root particle size/number density distribution), the average particle size for this time period was 4 micrometers.

Based on the assumed particle size distribution, the theoretical calibration curve of Figure 41 was used to convert laser light extinction to dust concentration. The results are given in Figure 42. In the absence of independent data on particle size distribution beyond 1 ms, the determination of the dust density beyond this time was not attempted.

4.3 DUST VELOCITY DATA AT CERF 6' SHOCK TUBE .

Fewer measurements were attempted at the 6' shock tube during the reporting contract. The results of the measurements for a series of nonprecursed dusty flows are reported in Figures 43 to 46. Here, the velocity measurements represent the same trend as those obtained in the smaller shock tube.

Figure 47 shows the velocity data for all the measurement heights. The development of a velocity boundary layer is apparent as early as 2 ms after the passage of the shock front. Figures 48 and 49 present the velocity profiles obtained from the velocity data. Also from the velocity data, Figure 50 shows the time of arrival of the dust particles at the various measurement heights. No measurement of the vertical velocity components were made in this facility.

Preliminary measurements of the dust velocity in precursed dusty flow was made. The dust velocities were found to be generally higher than those obtained for the nonprecursed flows.

SECTION 5
CONCLUSIONS

The measurements at both TRW's 4 x 4 inch shock tube and the CERF 6' shock tube were obtained at various points above the dust bed. It was shown that the particle velocity just behind the shock wave was not a strong function of the measurement height. The results, however, show the development of a boundary layer for both test sites at a laser time behind the shock wave. For the TRW data, the velocity profile was approximately similar to that of a turbulent boundary layer with a rough surface, following a power law with exponent values of 1/4 or 1/5. The results at the CERF 6' shock tube were similar with an exponent value approximately 1/4.

An attempt was made to estimate the density of the particles at some positions in the flow for the 4 inch shock tube at TRW. Simultaneous measurements of the laser light extinction was made. This information along with assumptions on the particle size distribution generated the data on the particle concentration behind the moving shock wave.

SECTION 6

LIST OF REFERENCES

1. D. R. Ausherman, "Initial Dust Lofting Shock Tube Experiments", DNA Report #31627, 1973.

2. D. Modarress, "Transient Velocity Measurement in Dusty Boundary Layer Developed Behind a Shock Wave", Presented at the Winter Annual Meeting of the American Society of Mechanical Engineers, Miami Beach, Florida, November 17-22, 1985.

3. D. Modarress, H. Tan, "LDA Signal Discrimination in Two-Phase Flows," Experiments in Fluids, 1, 129-134, 1983.

4. Proceeding, "Hard Mobile Launchers Simulation Working Group Meeting", R&D Associates, Marina Del Rey, 17 October, 1984.

5. R. Weurker, R. Batt, K. Magiawala, and I. Cohen, Engineering Research Support to Defense Nuclear Agency ICB Basing Program, Volume 4, Instrumentation Development", Final Report, DNA001-84-C-0107.

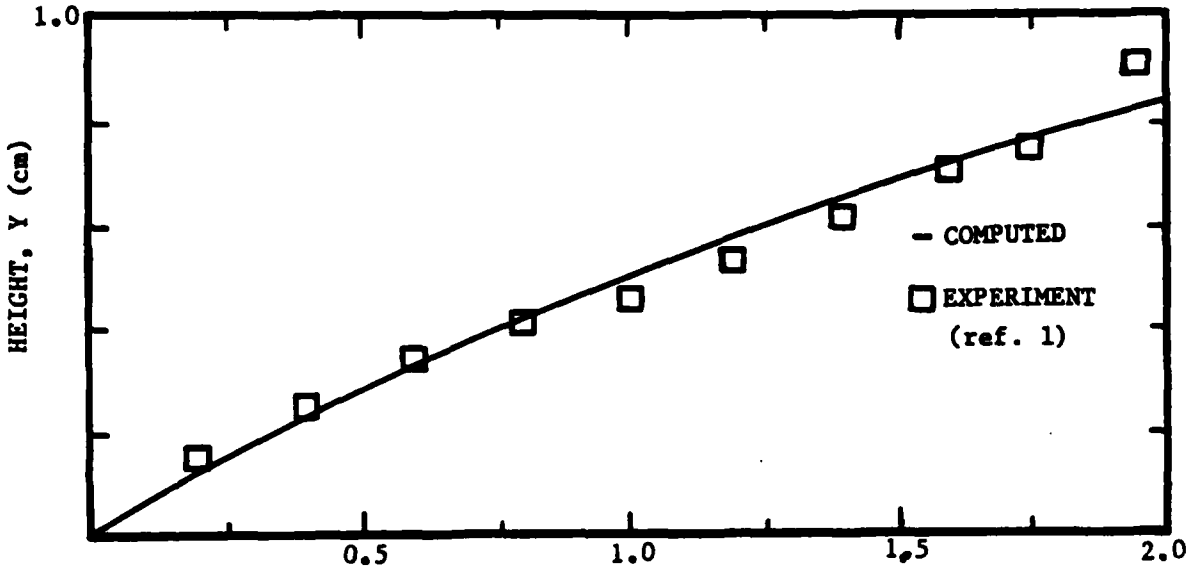

Figure 1. Initial Trajectory.

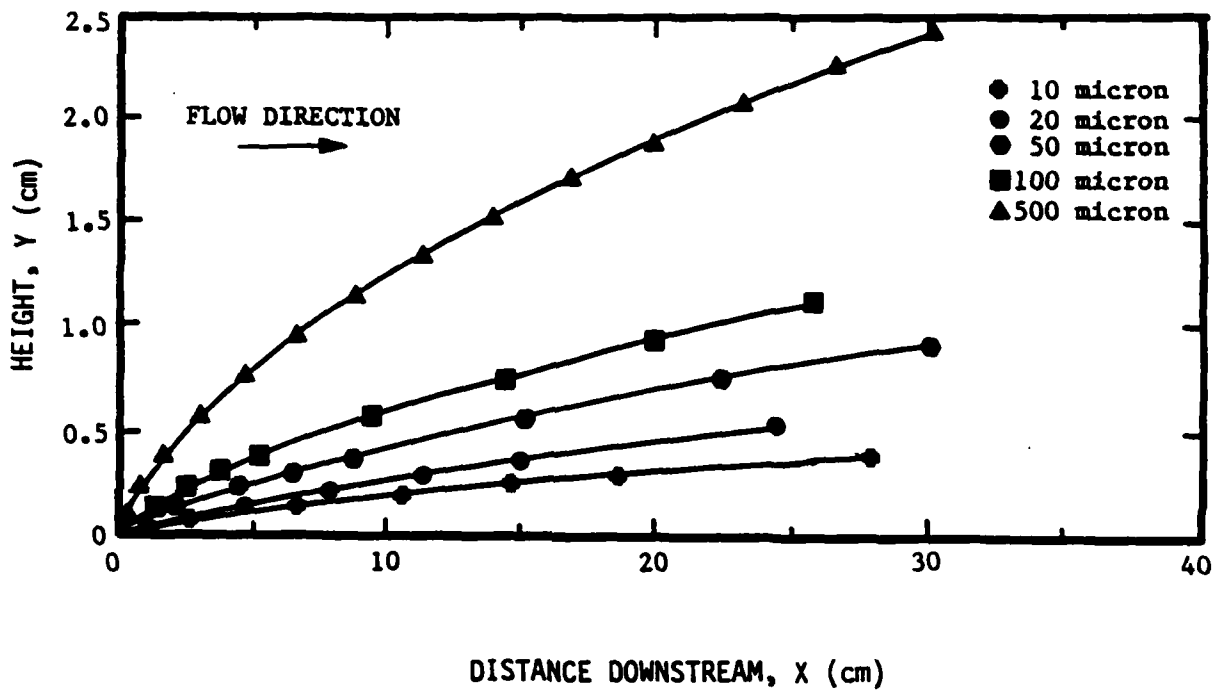

Figure 2. Particle Trajectory.

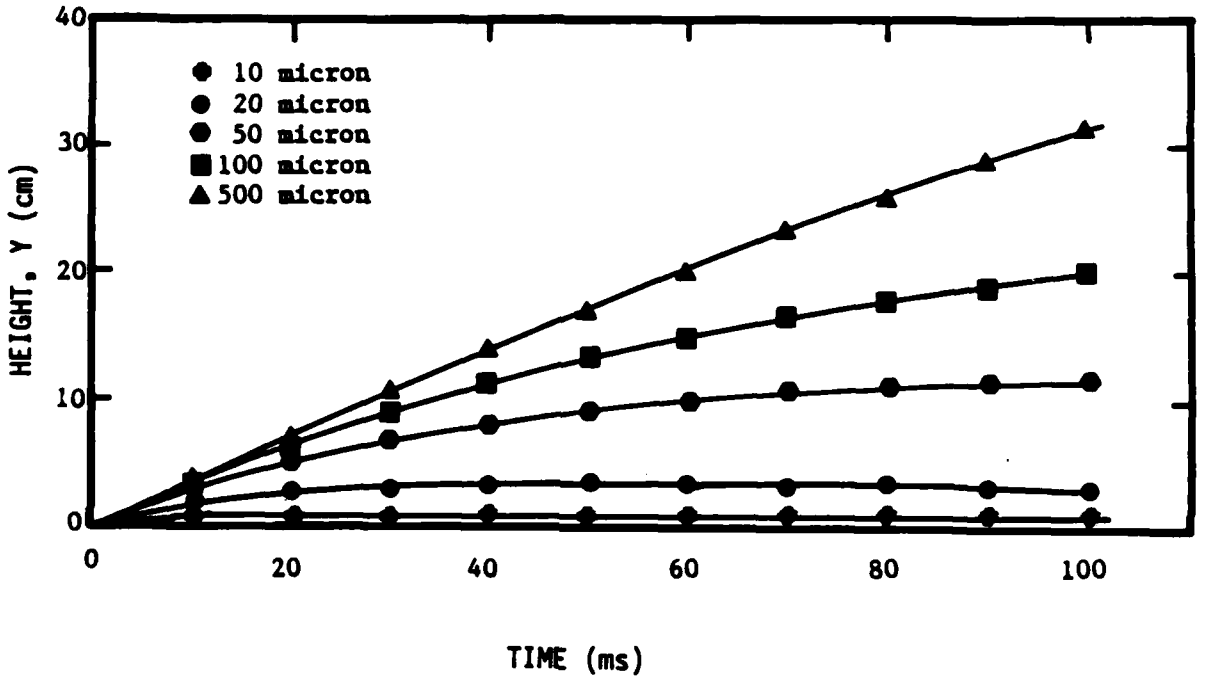

Figure 3. Particle Elevation.

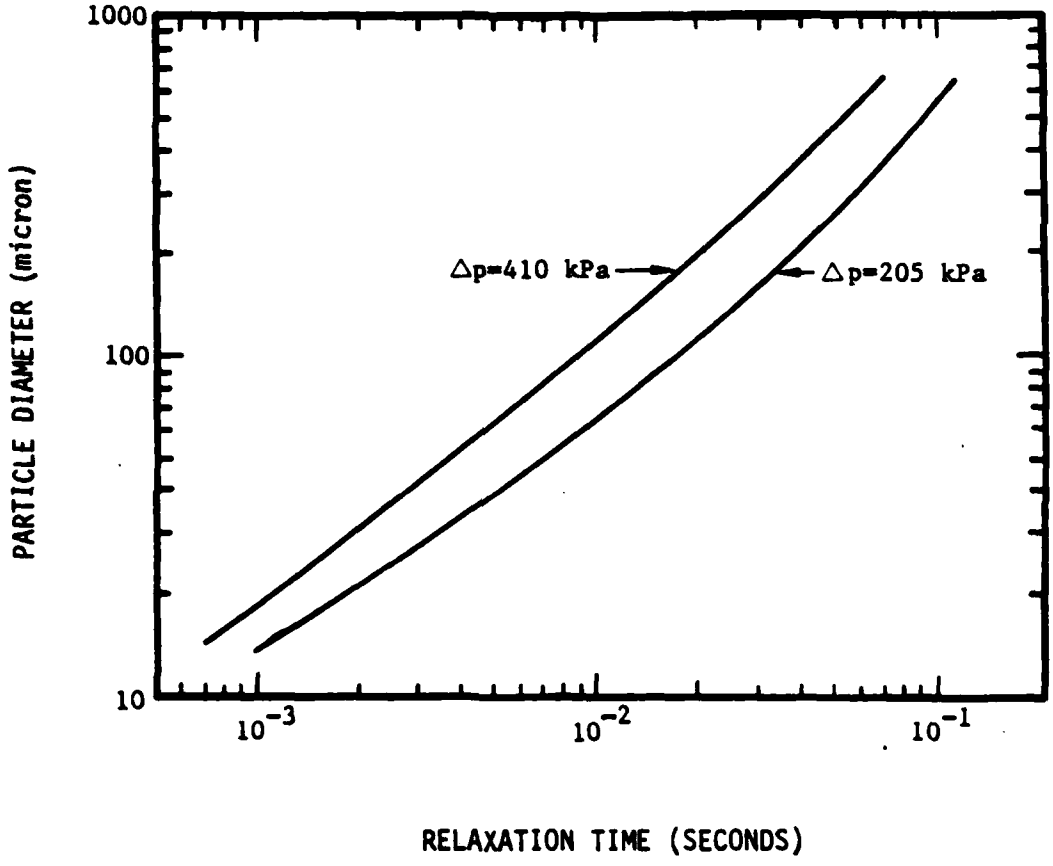

Figure 4. Particle Relaxation Time.

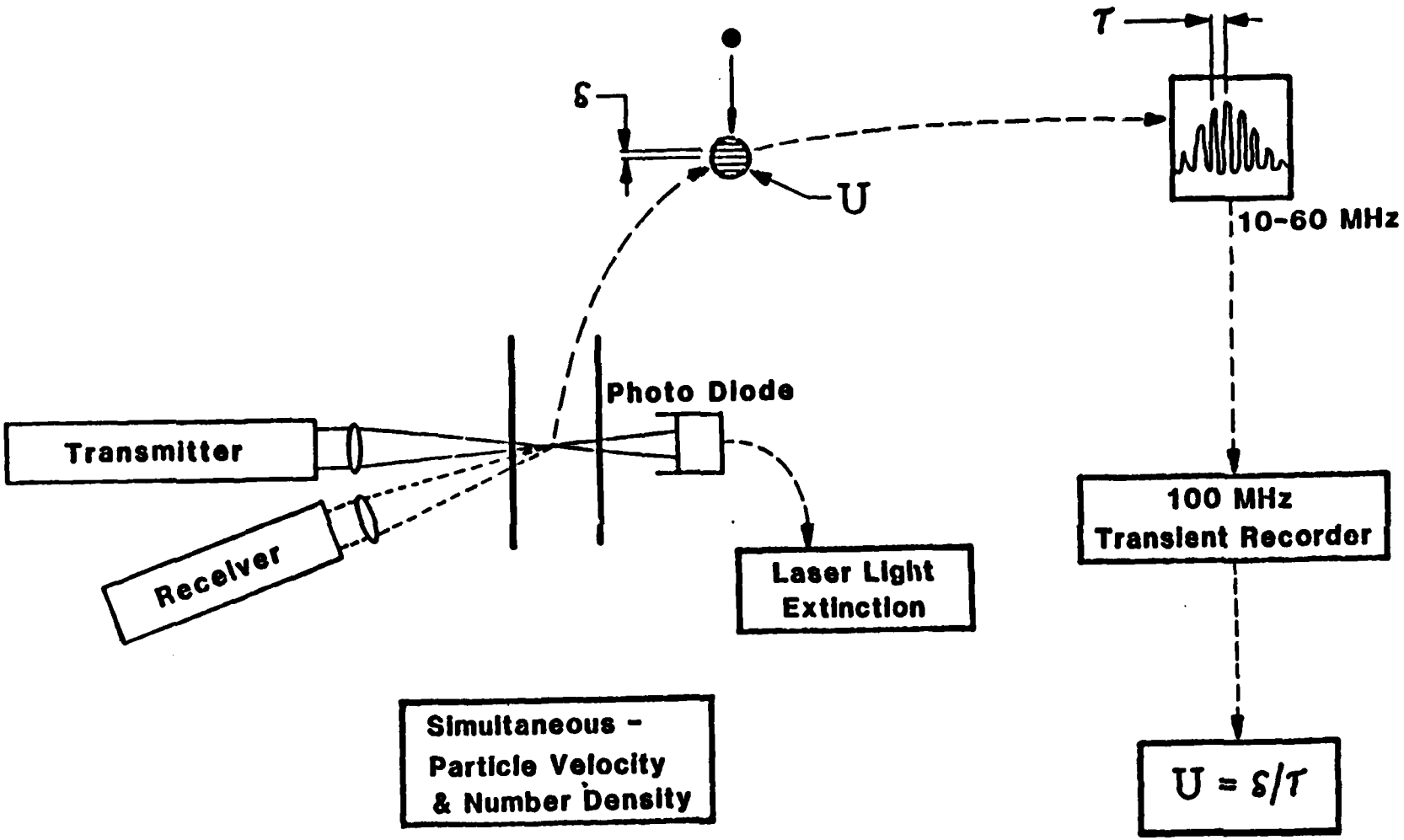

Figure 5. Principle of Operation.

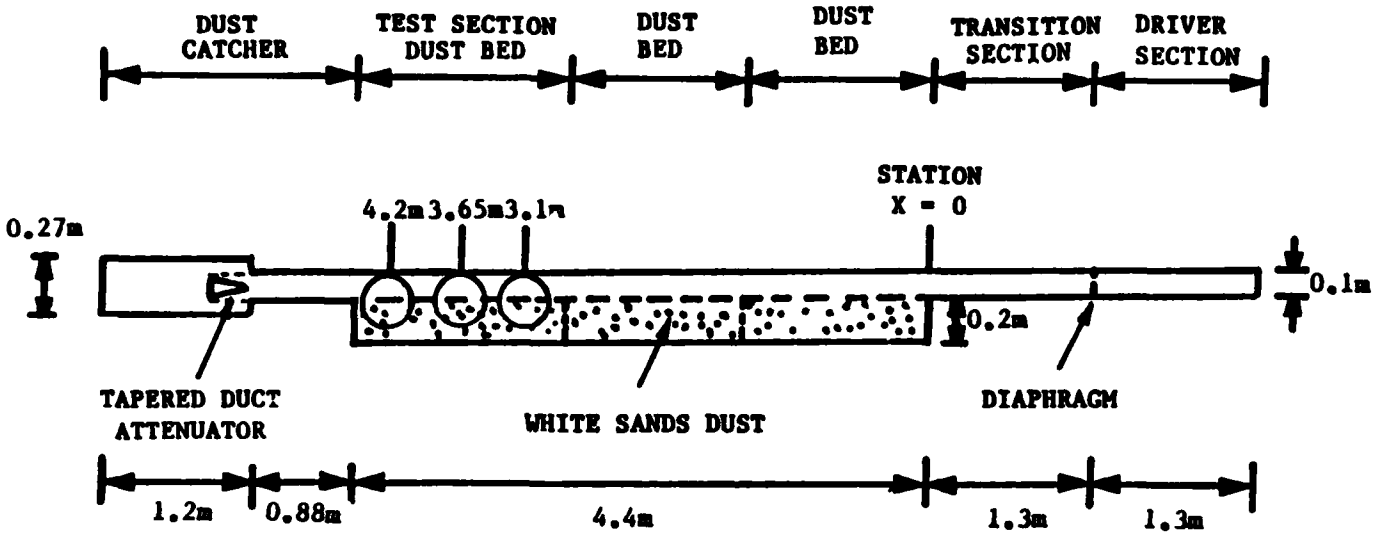

Figure 6. Schematic of 4 x 4 Inch Shock Tube Facility at TRW.

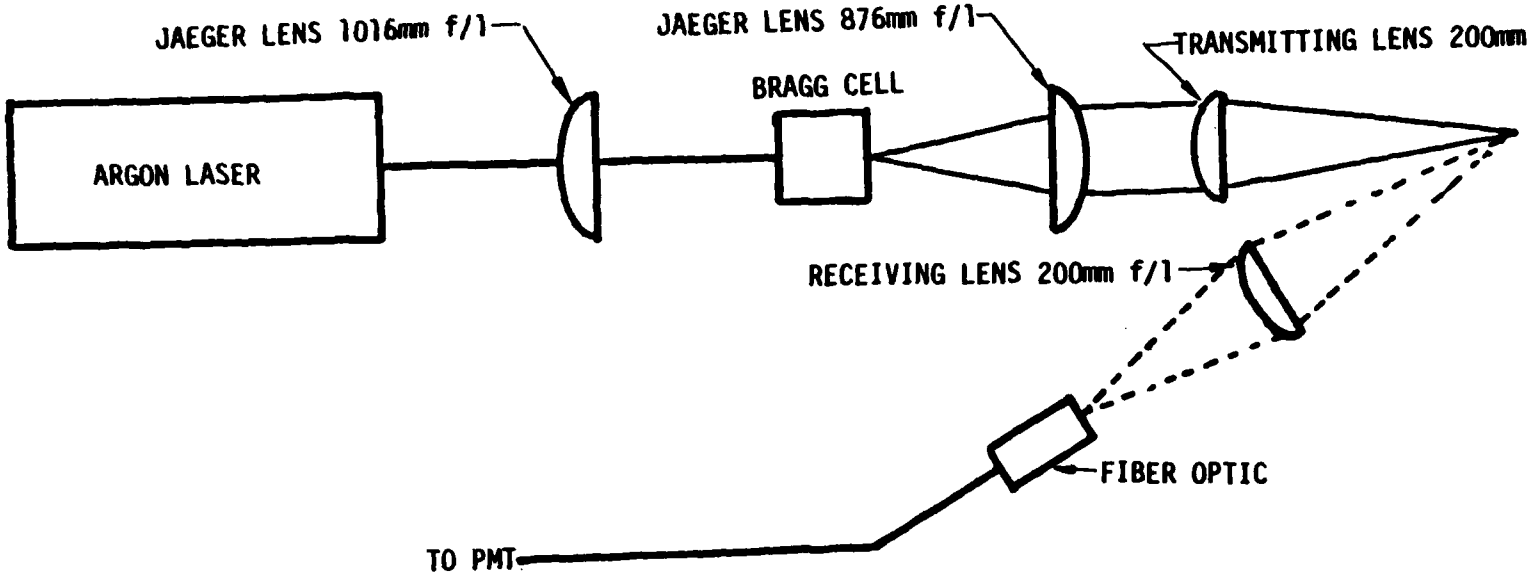

Figure 7. Schematic of Single Component Laser Velocimeter for TRW Shock Tube.

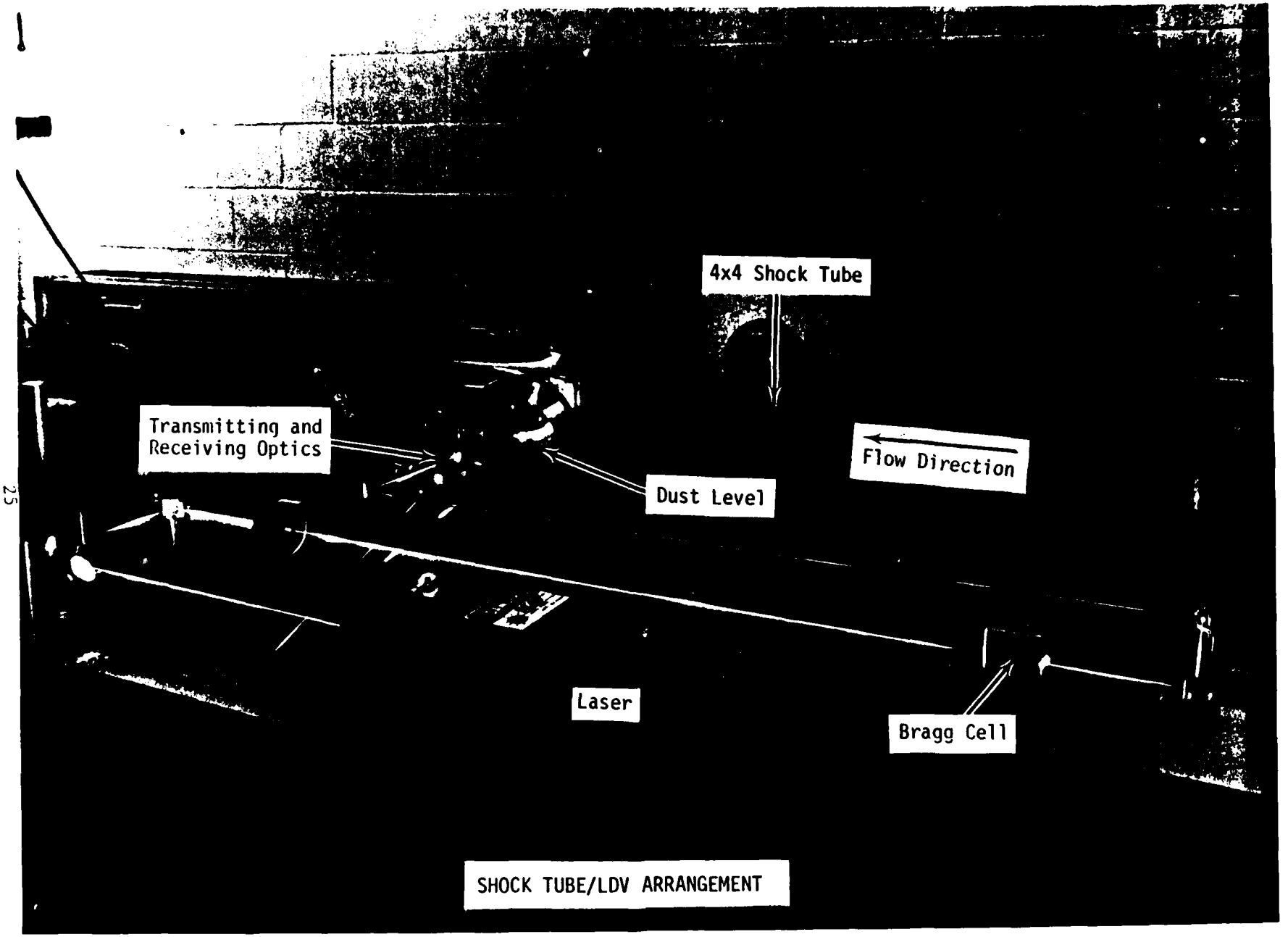

Figure 8. Arrangement of Laser Velocimeter at 4 x 4 Inch Shock Tube.

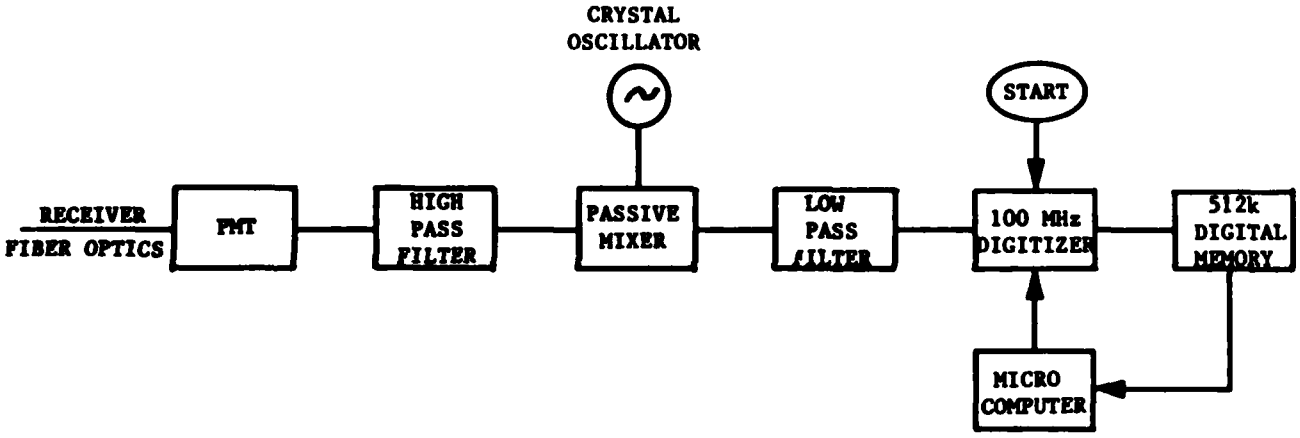

Figure 9. Block Diagram of the Data Acquisition System.

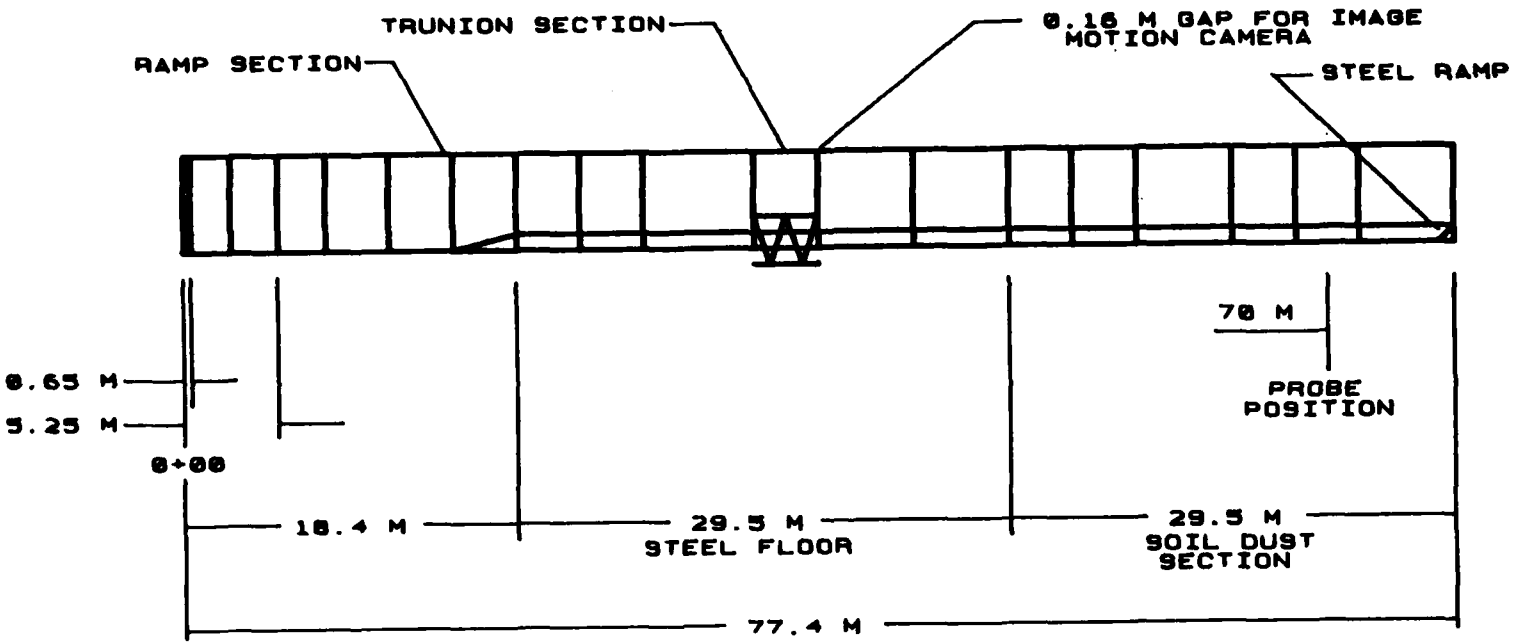

Figure 10. Schematic of 6-Foot Shock Tube Facility at CERF.

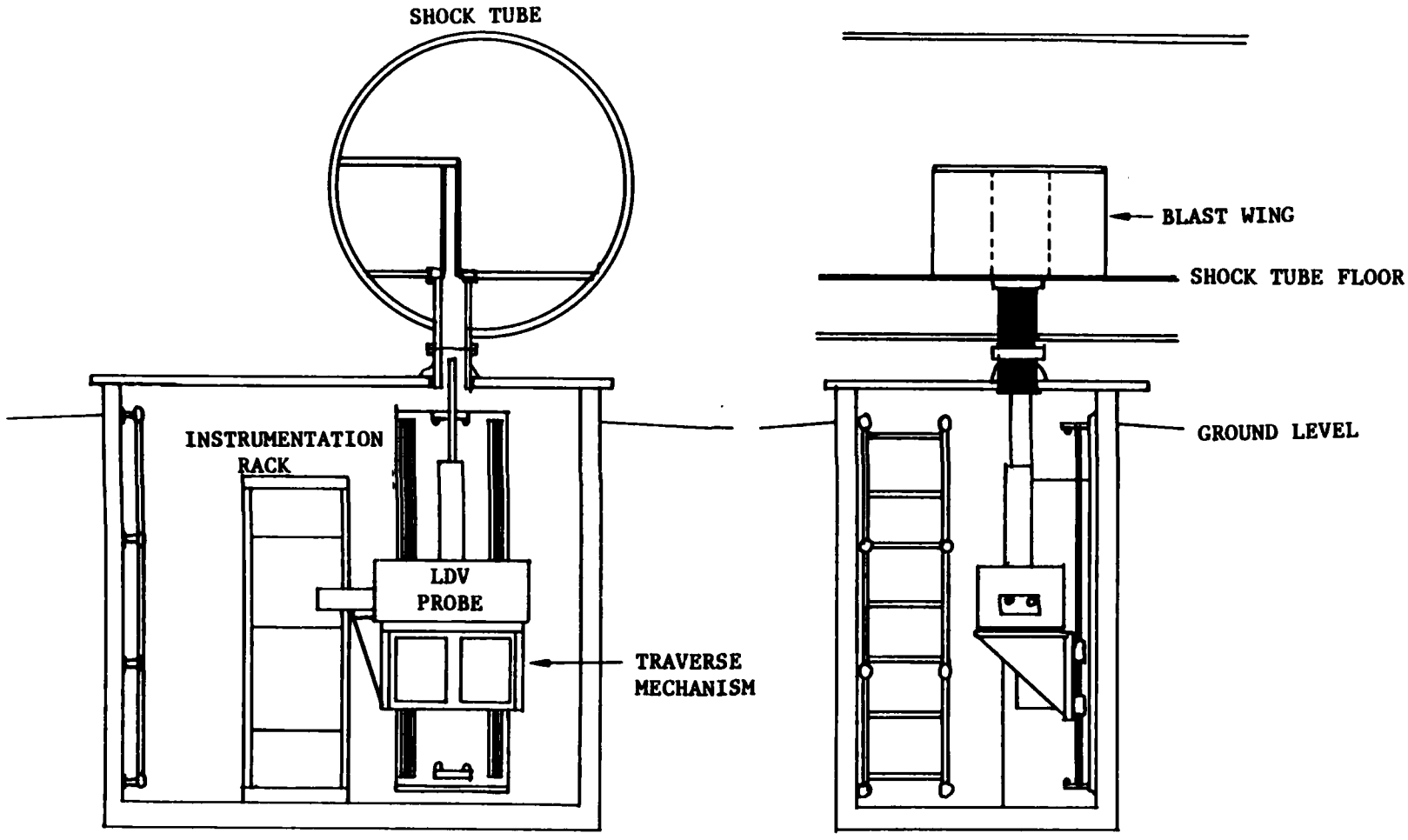

Figure 11. Laser Velocimeter Installation at CERF 6' Shock Tube.

Figure 12. Traversing Mechanism Inside the Vault.

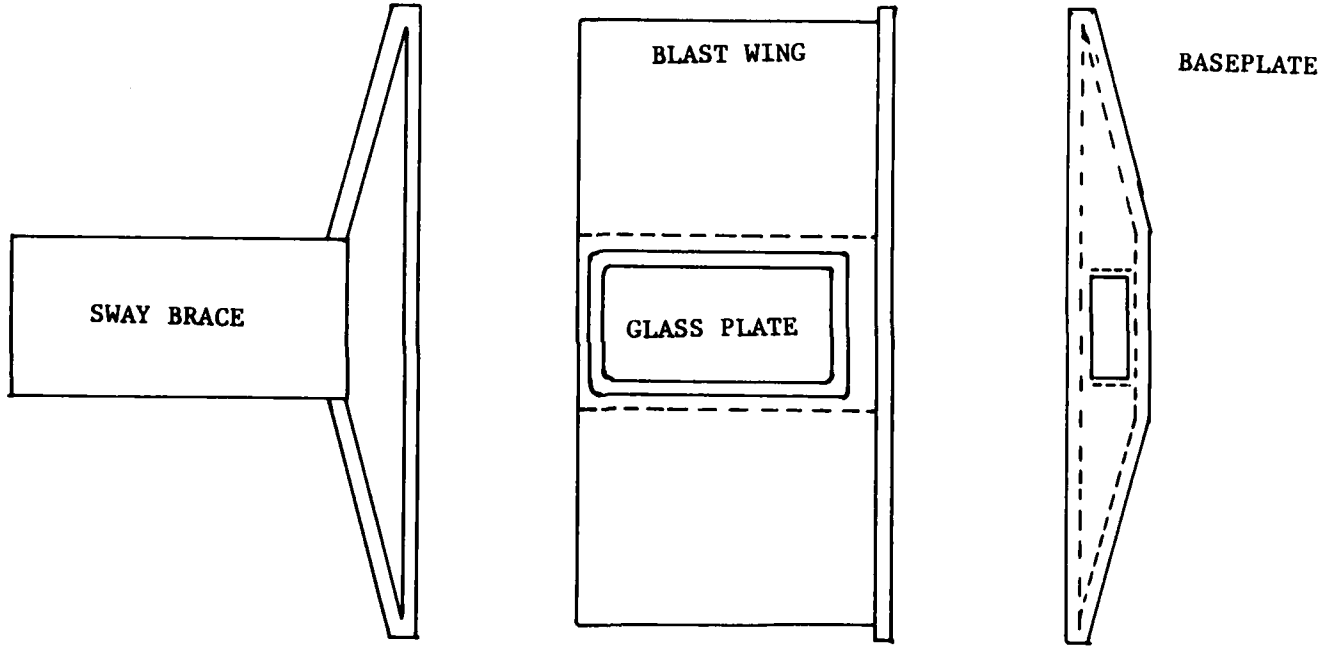

Figure 13. Schematic of the Blast Wing.

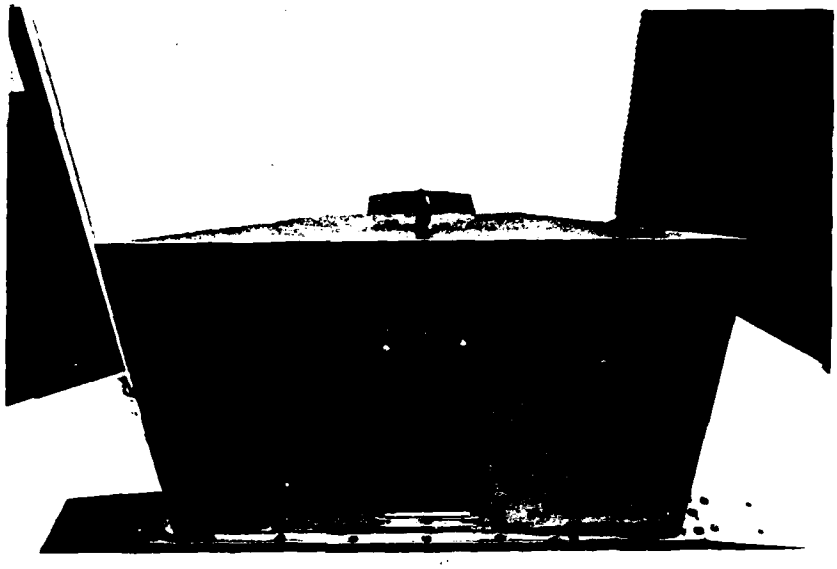

Figure 14. Blast Wing for Installation at the 6' Shock Tube.

Figure 15. Instrumentation Vault.

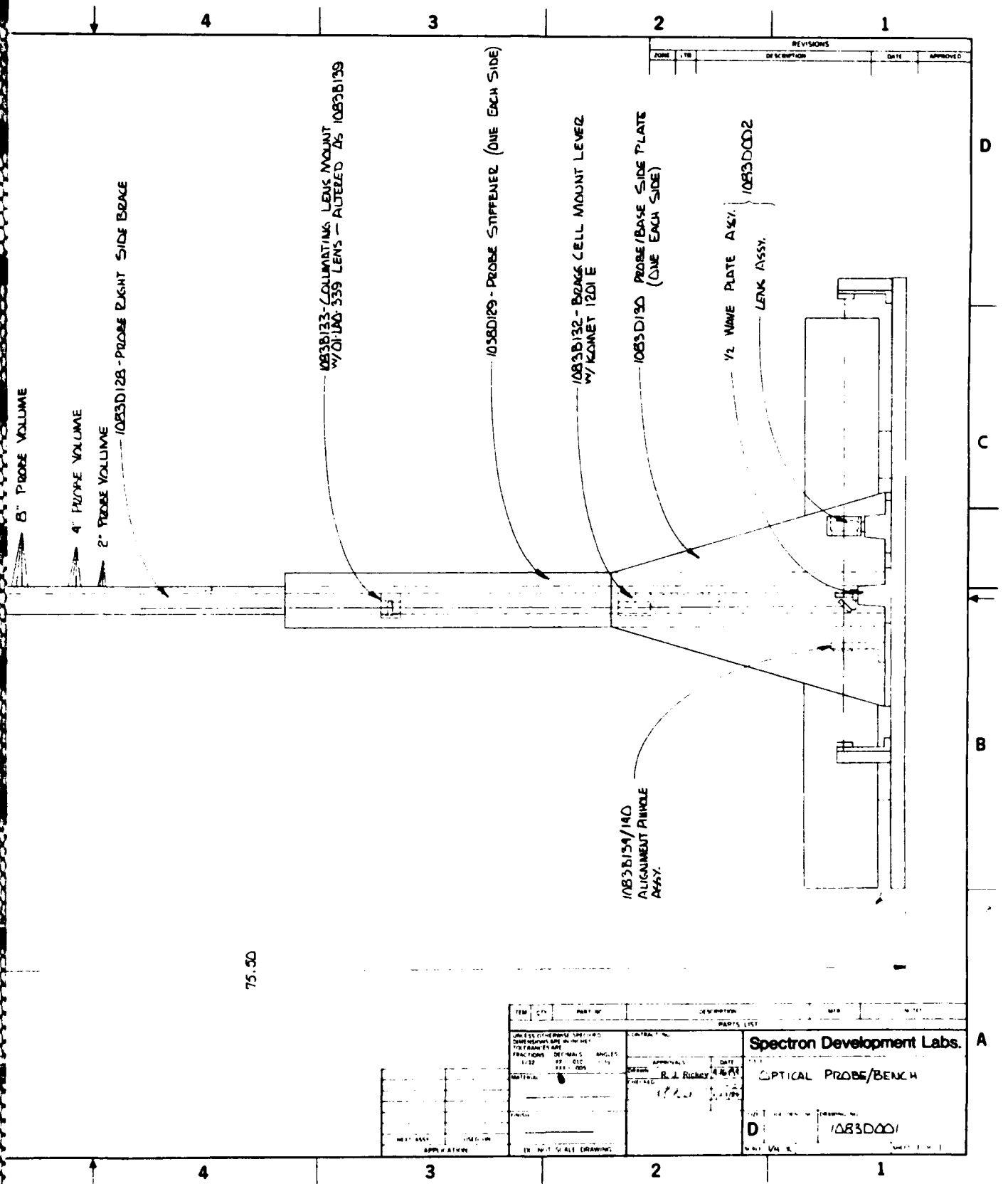
4
3
2
1
D
C
B
A
8" PROBE VOLUME
4" PROBE VOLUME
2" PROBE VOLUME
1083D128 - PROBE RIGHT SIDE BRACE
1083B133 - COLLIMATING LENS MOUNT W/ OPTICAL 339 LENS — ALTERED AS 1083B139
1083B129 - PROBE STIFFENER (ONE EACH SIDE)
1083B132 - BEAM CELL MOUNT LEVER W/ KOMET 1201 E
1083D130 PROBE/BASE SIDE PLATE (ONE EACH SIDE)
½ WAVE PLATE ASSY.
1083D002
LENS ASSY.
1083B134/140 ALIGNMENT PINHOLE ASSY.
75.50
REVISIONS
PARTS LIST
Spectron Development Labs.
OPTICAL PROBE/BENCH
R. J. Richey
D
1083D001

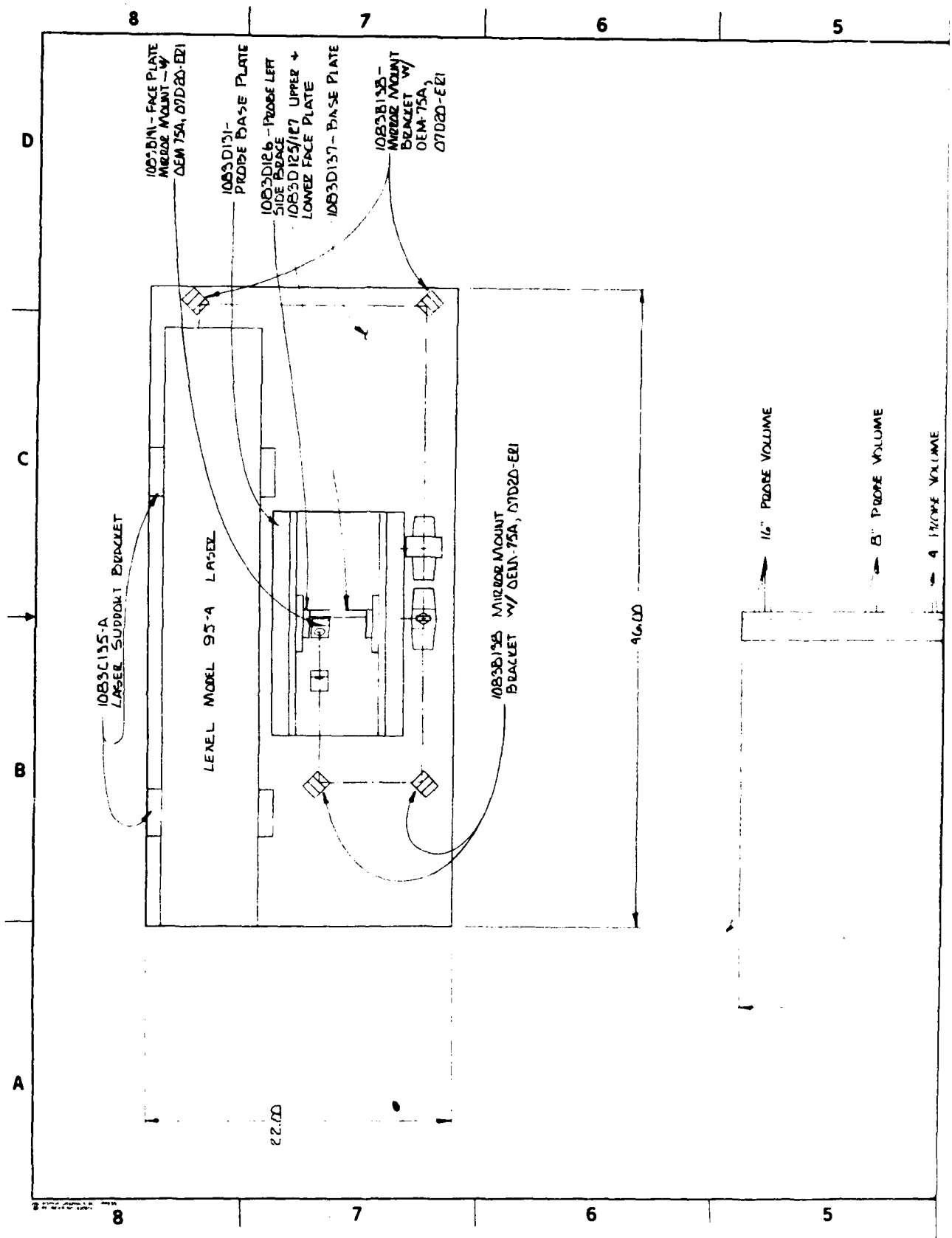

Figure 16. Optical Probe at CERF 6' Shock Tube.

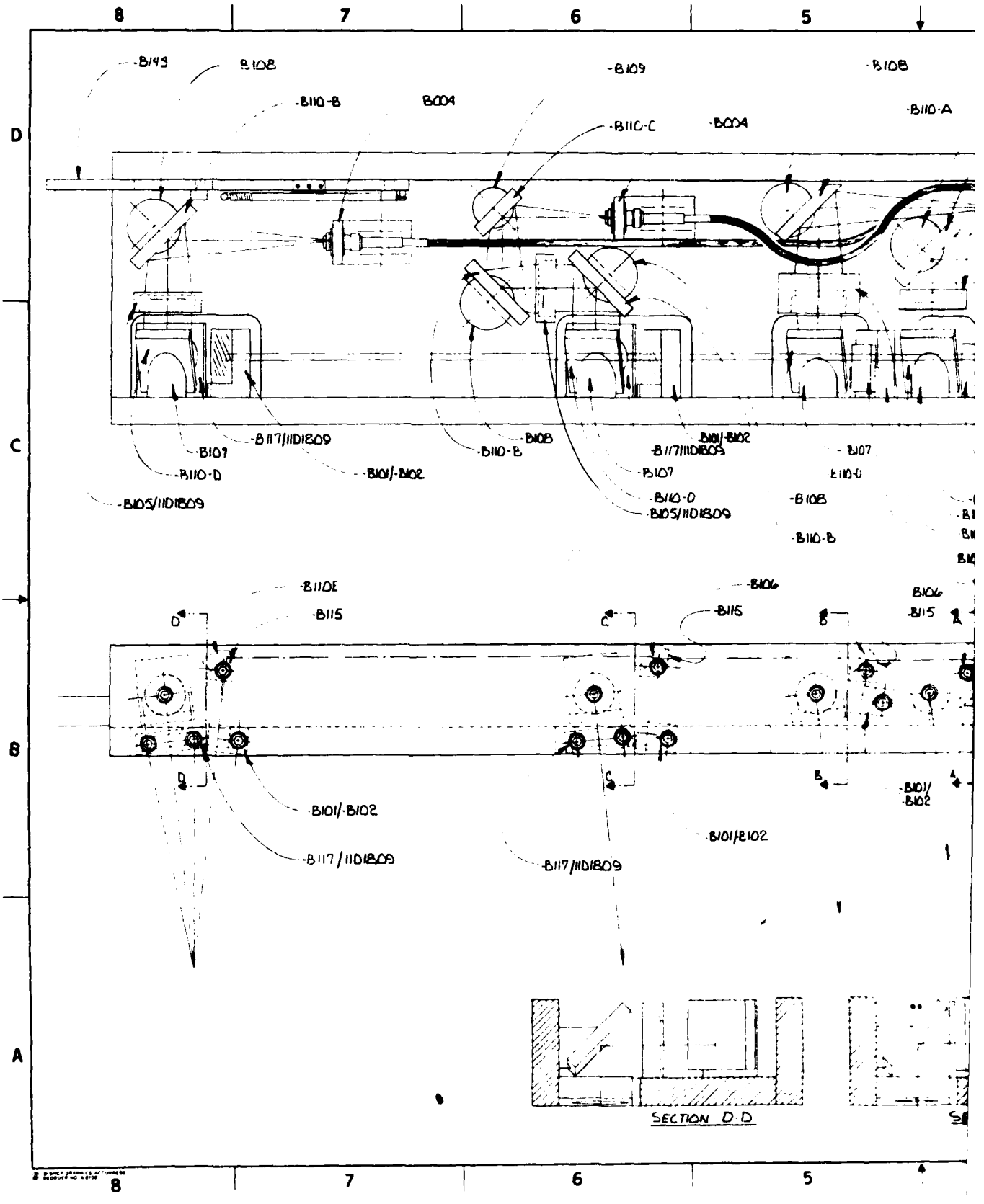
8
7
6
5
D
C
B
A
B109
B108
B110-B
B004
B110-C
B004
B110-A
B107
B117/11D1809
B110-D
B101/B102
B105/11D1809
B108
B110-B
B101/B102
B117/11D1809
B107
B110-D
B105/11D1809
B108
B110-B
B110E
B115
B106
B115
B106
B115
B101/B102
B117/11D1809
B101/B102
B117/11D1809
B101/
B102
SECTION D-D

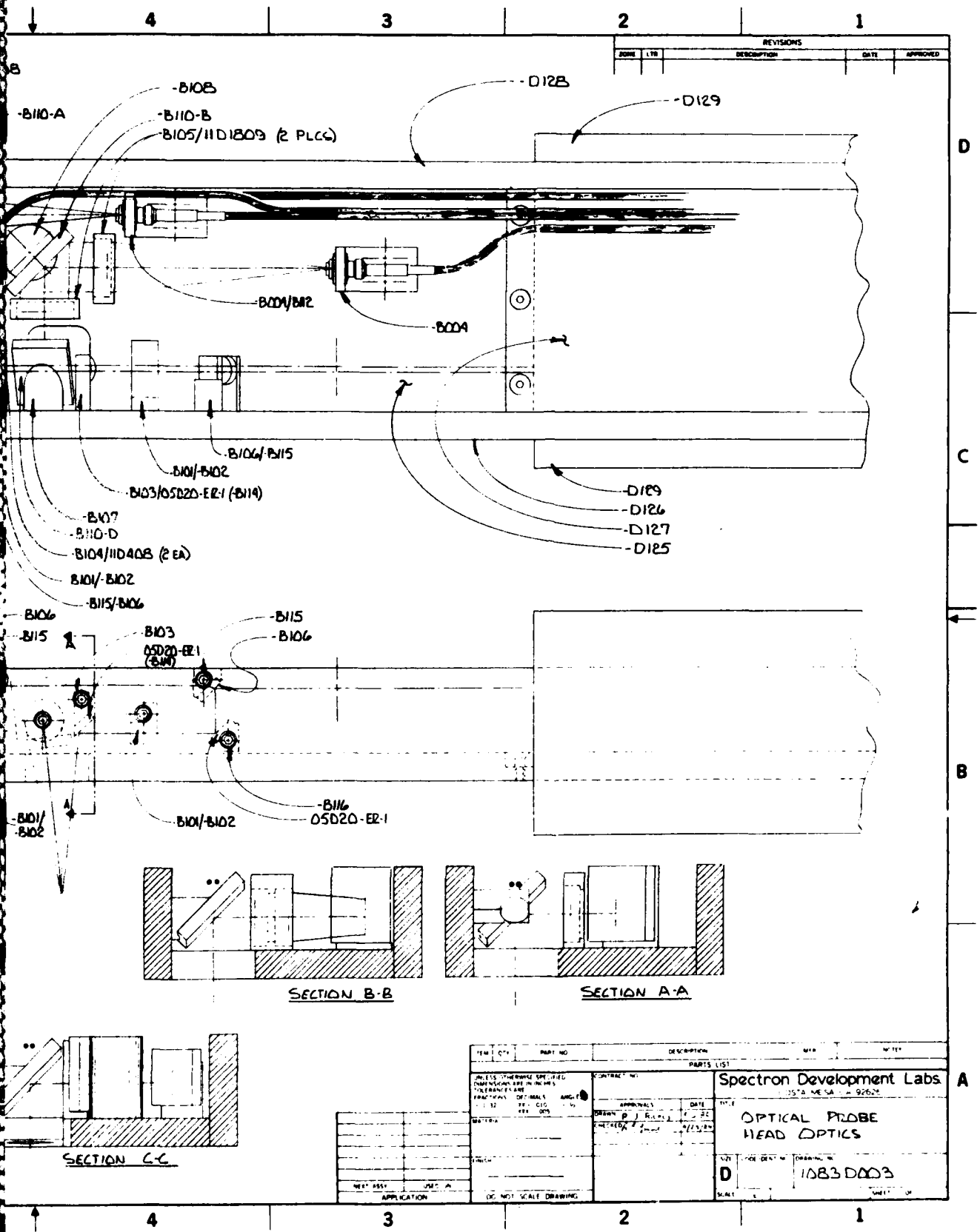

Figure 17. Detailed Schematic of Optical Assembly at CERT 6' Shock Tube.

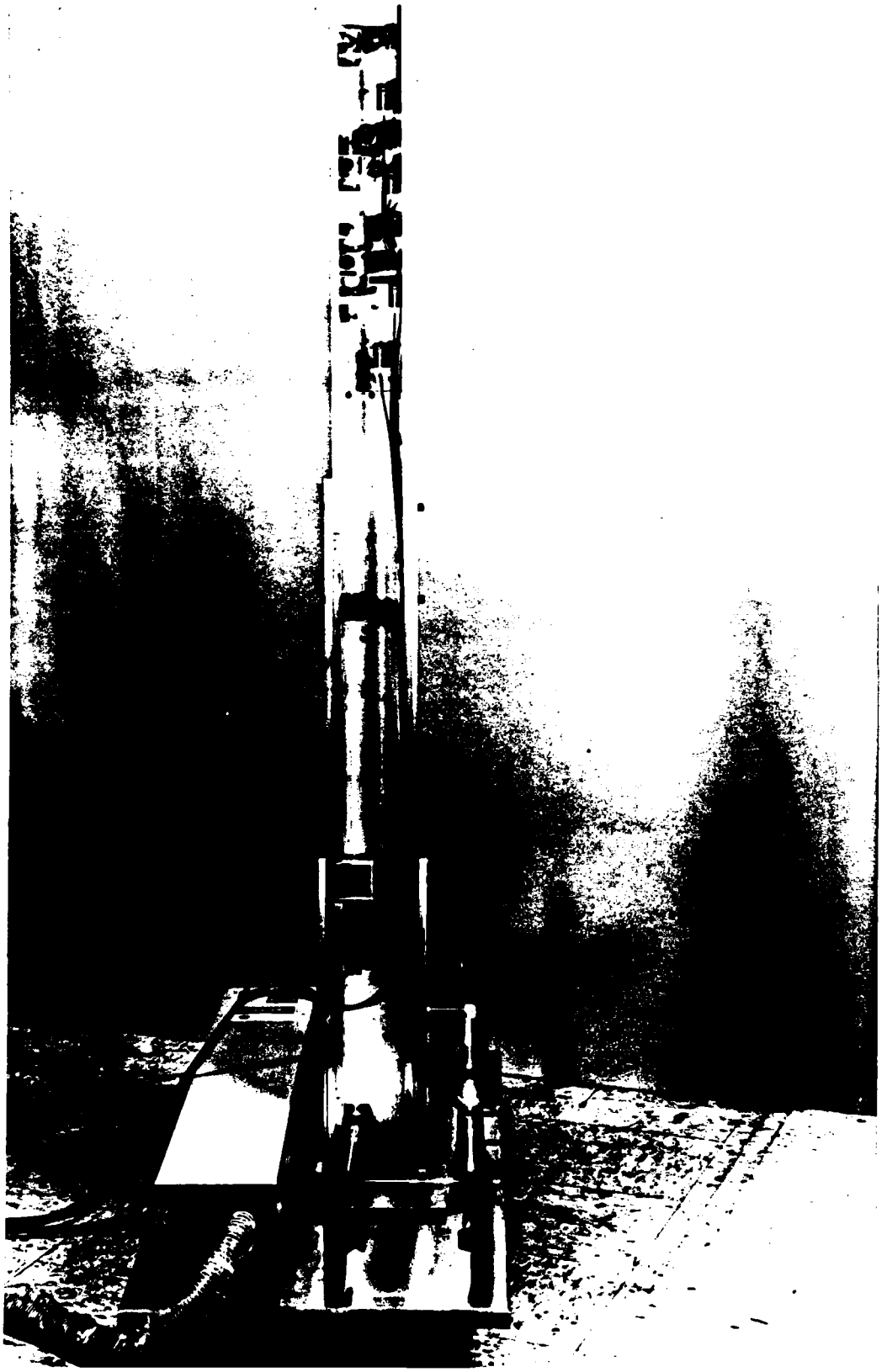

Figure 18. Photograph of Optical Probe at CERF 6' Shock Tube.

Figure 19. Photograph of Optical Head Assembly at CERF 6' Shock Tube.

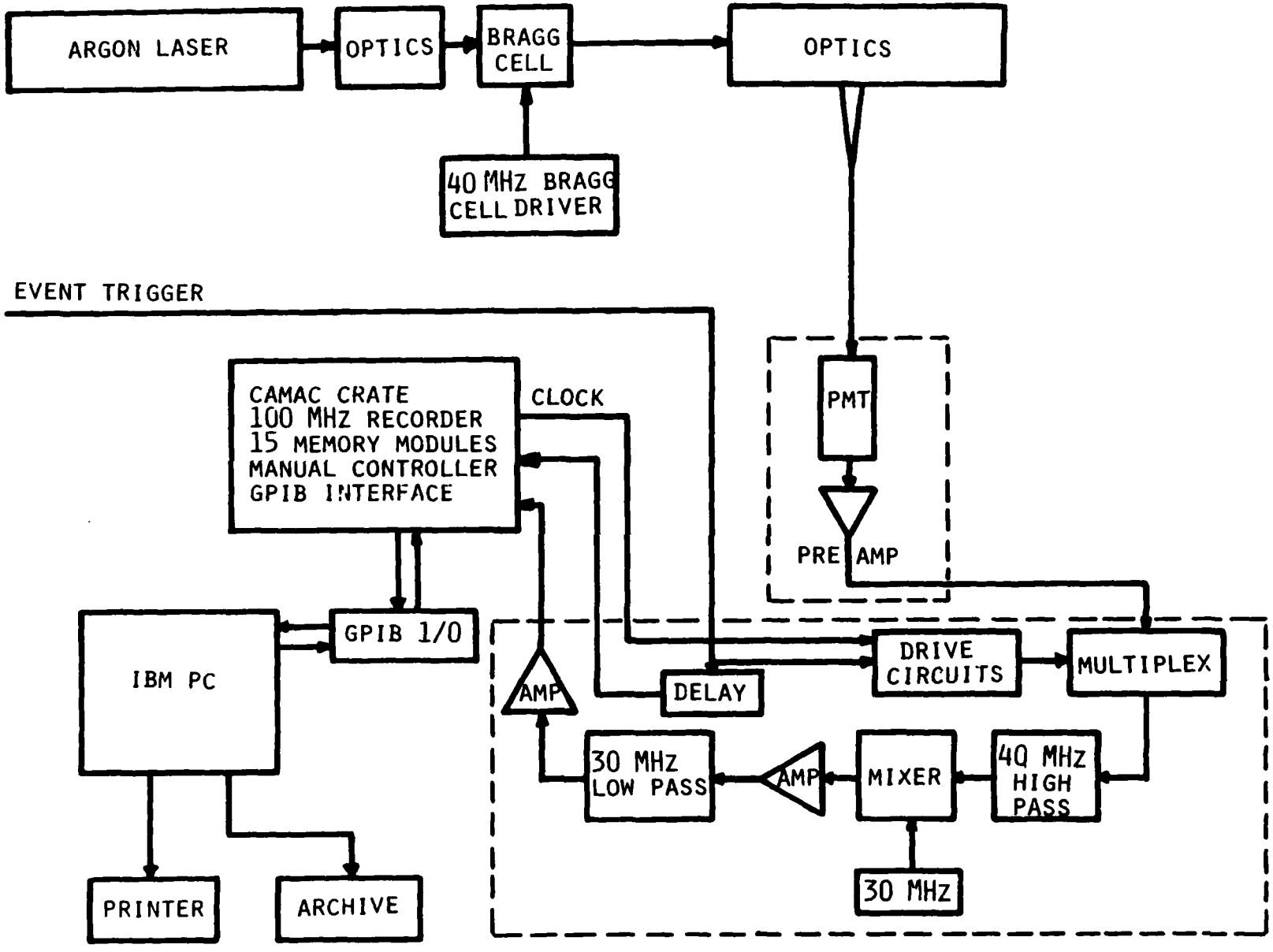

Figure 20. System Diagram for Laser Velocimeter at CERF 6' Shock Tube.

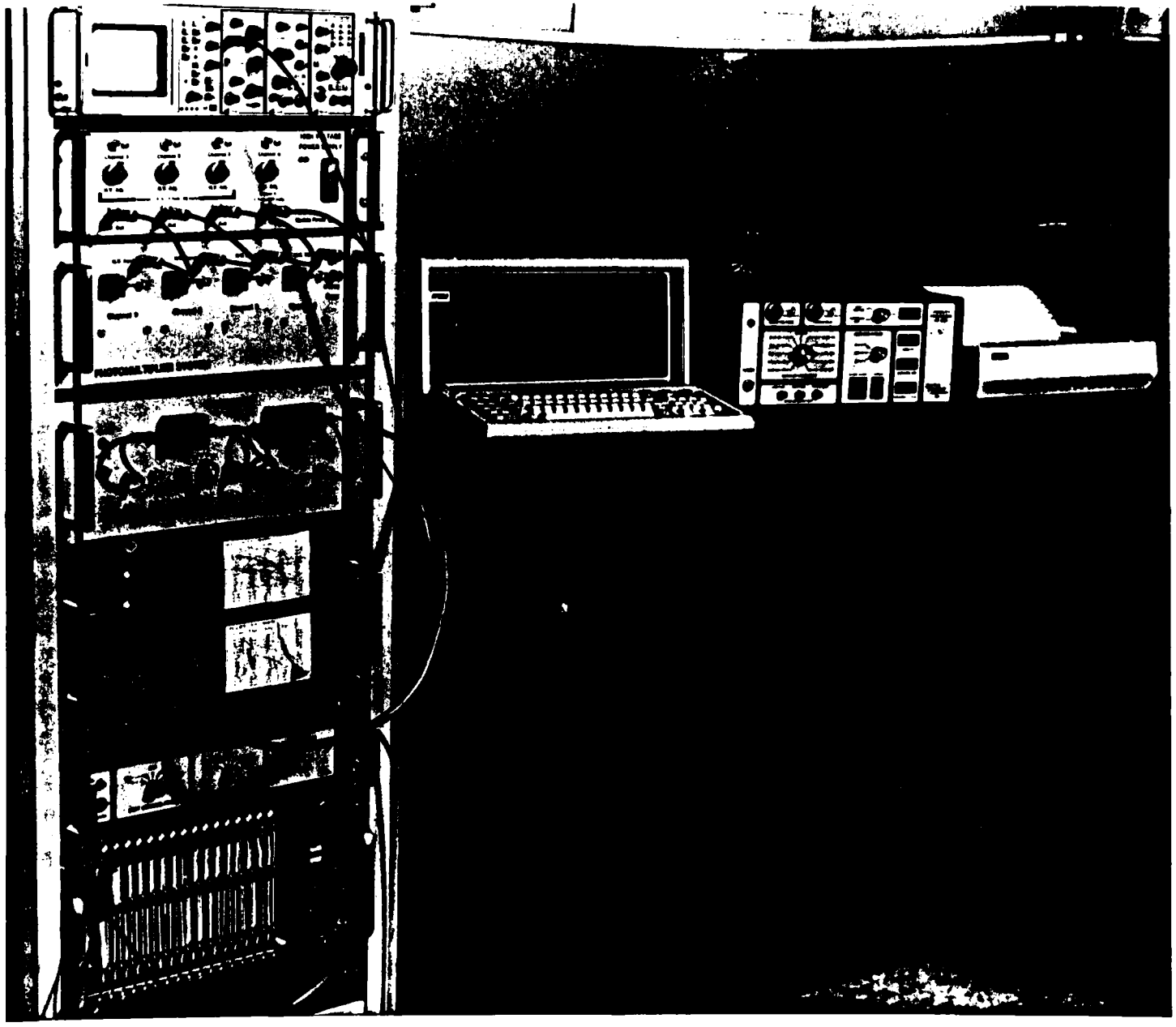

Figure 21. Photography of Electronic System for CERF 6' Shock Tube.

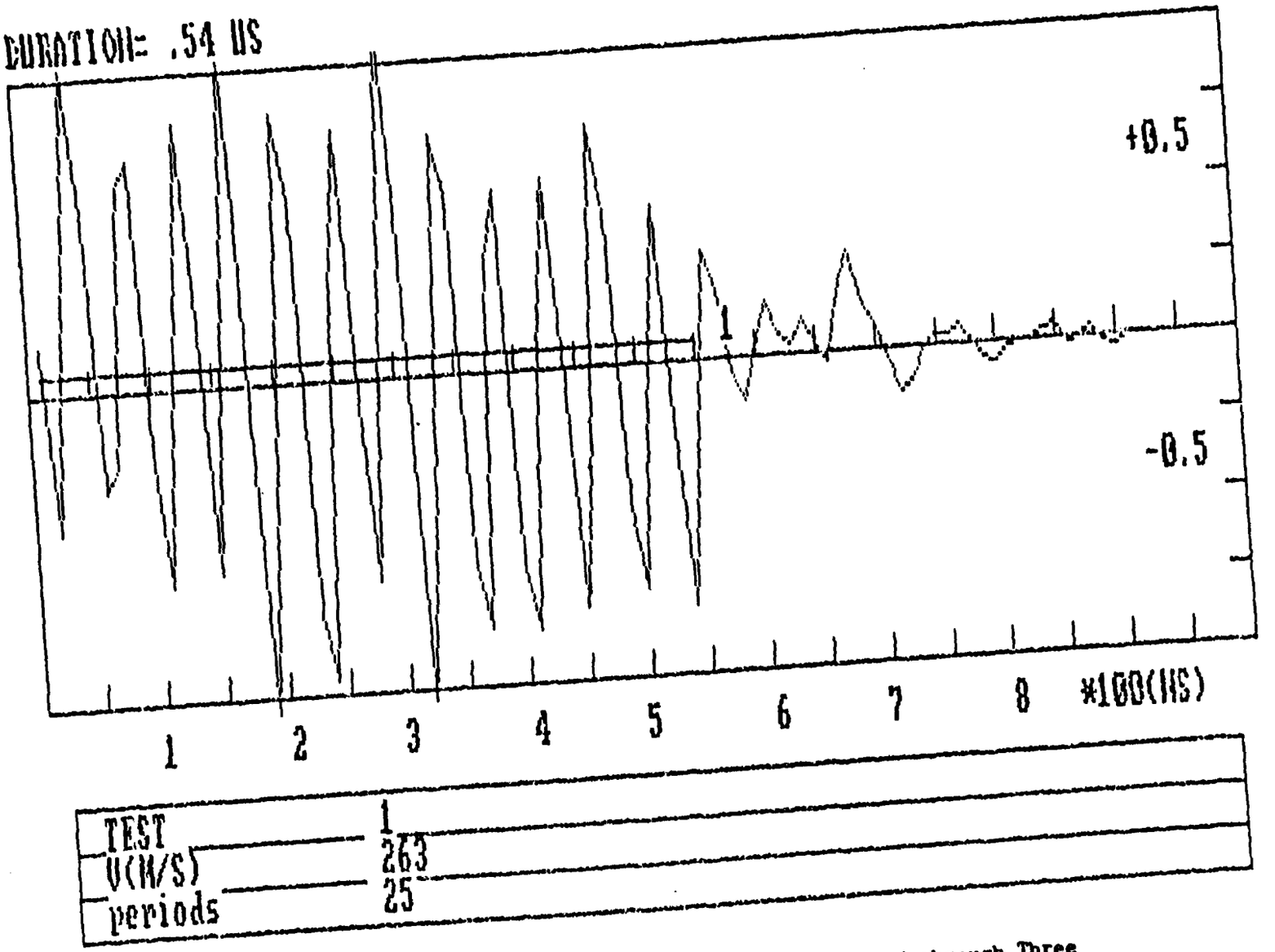

Figure 22. Record of a Typical Doppler Burst Processed through Three Level Comparator.

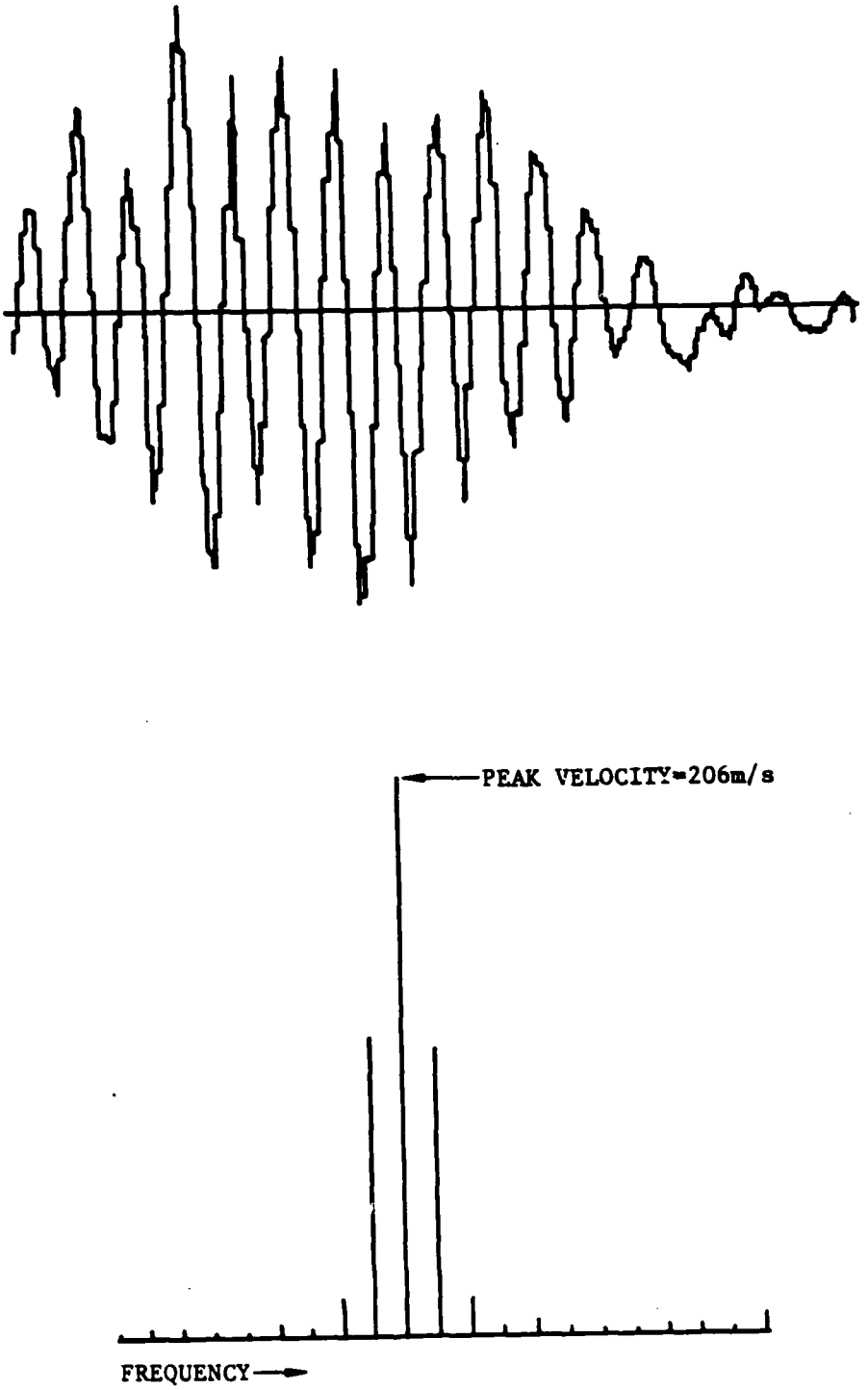

Figure 23. Record of a Typical Burst Processed through Spectrum Analysis.

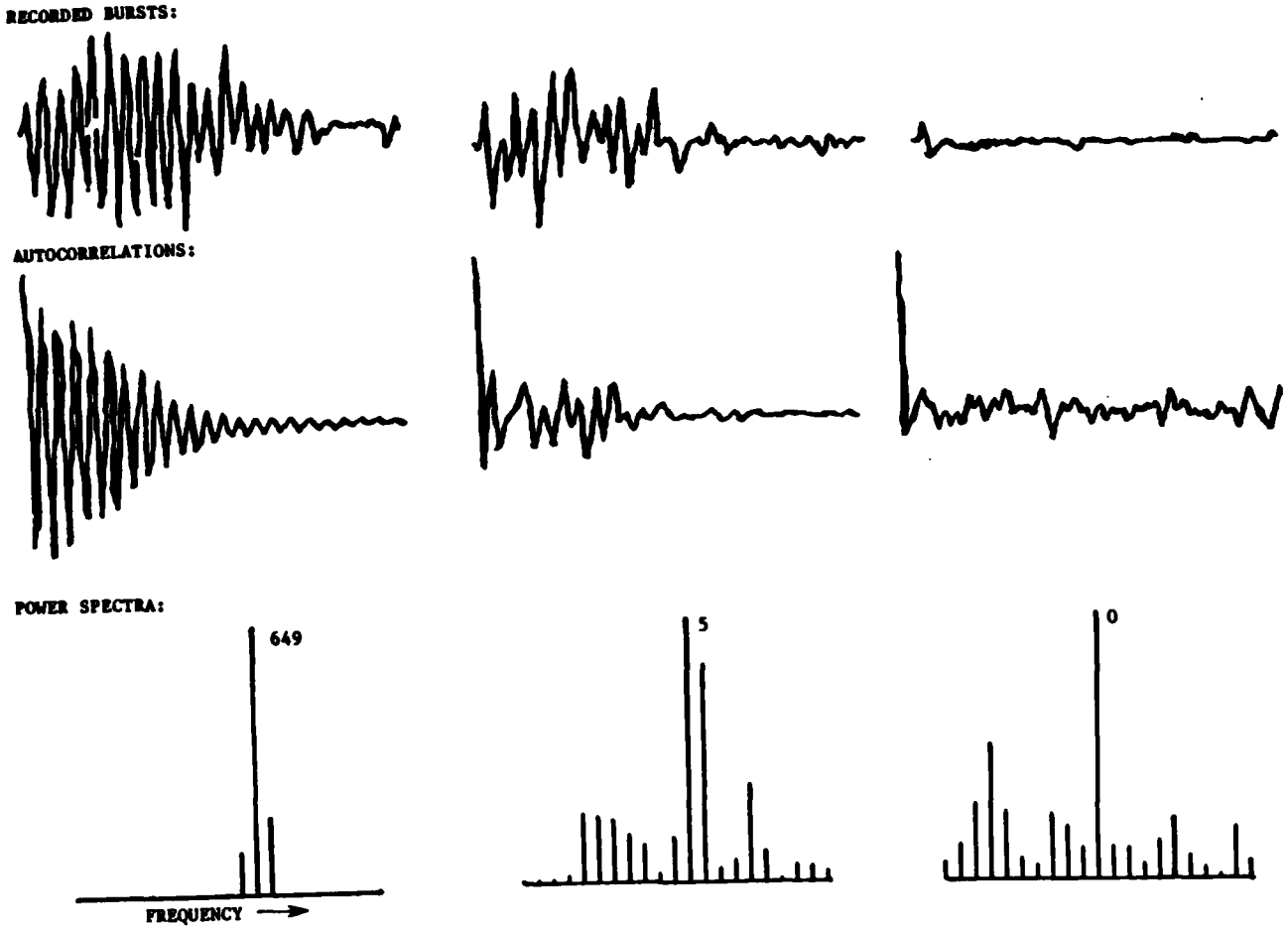

Figure 24. Individual Burst Power Spectra.

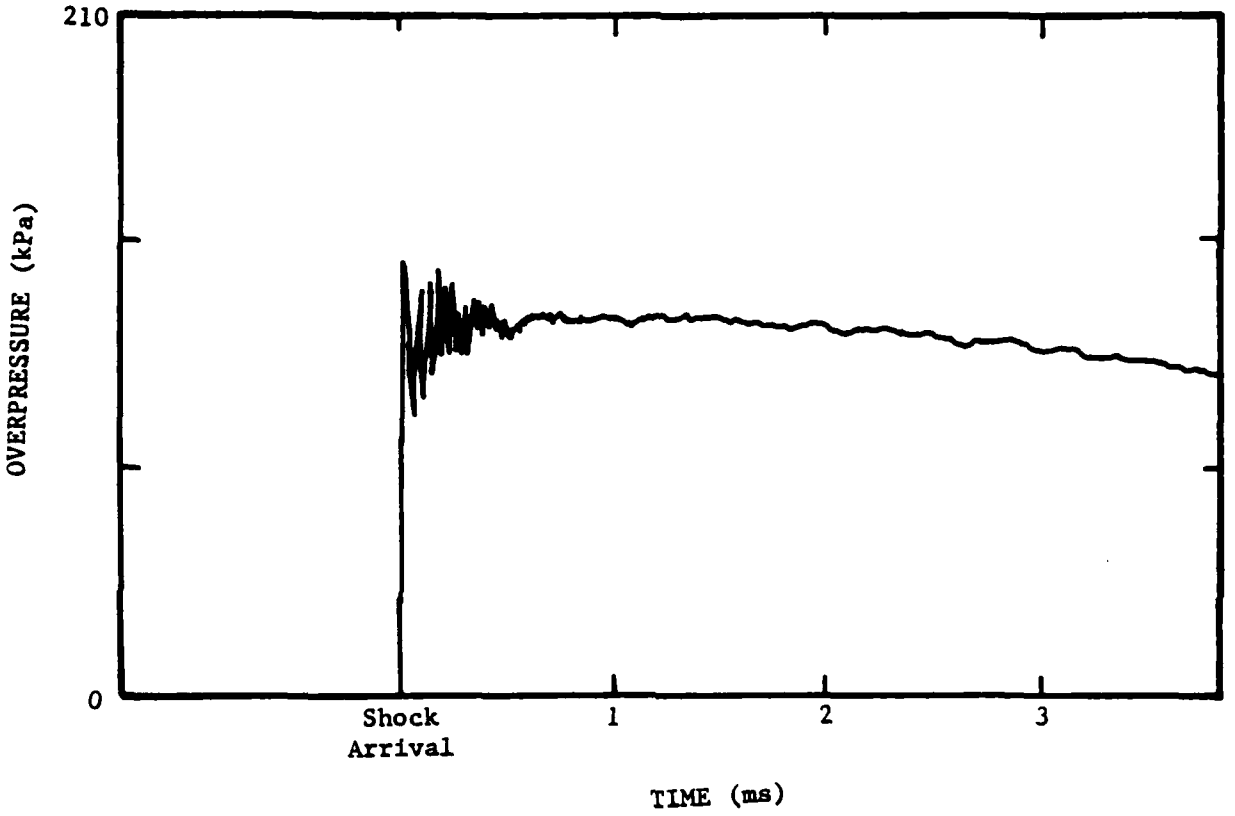

Figure 25. Pressure Time History at TRW 4" Shock Tube.

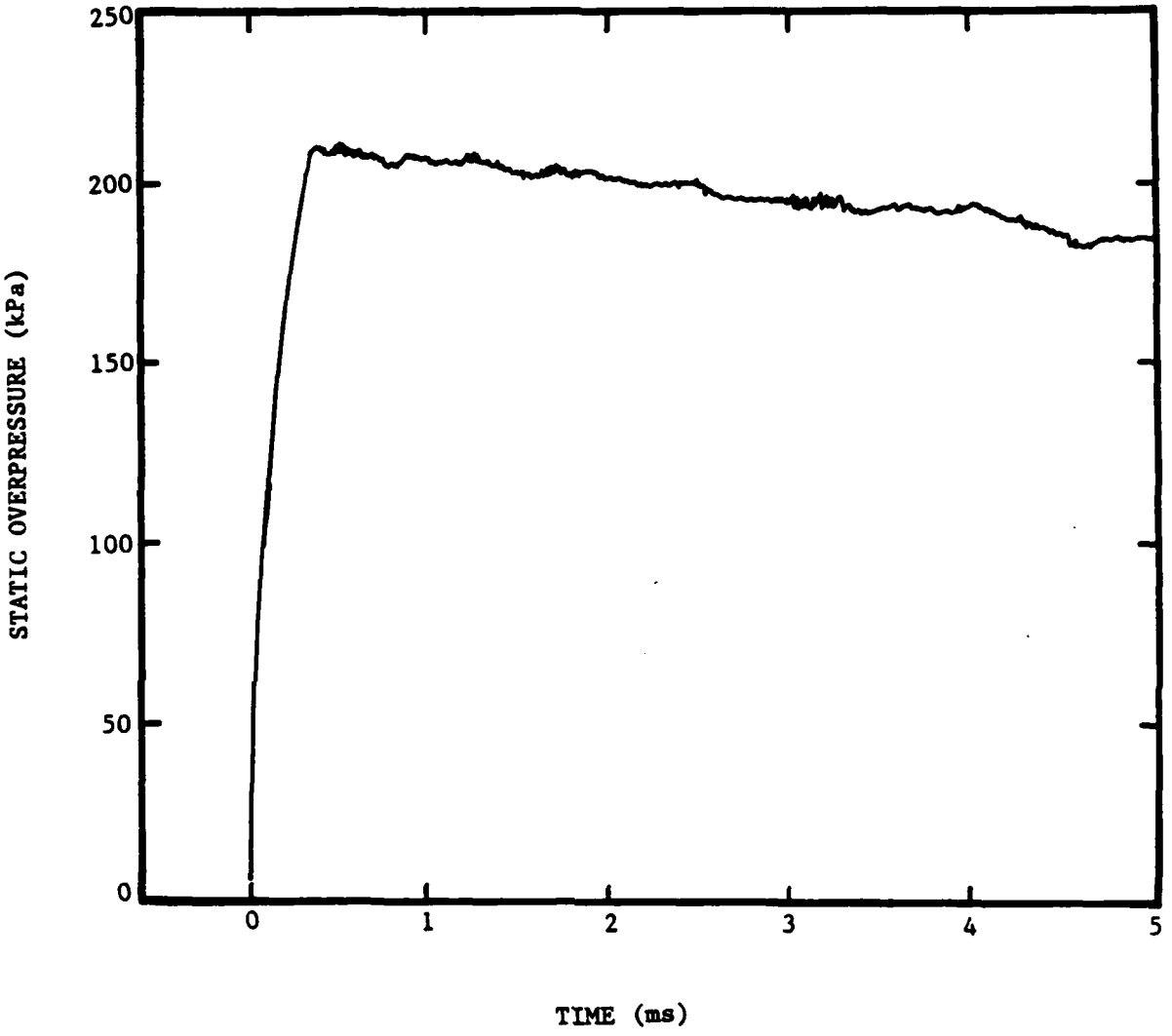

Figure 26. Pressure Time History at CERF 6' Shock Tube.

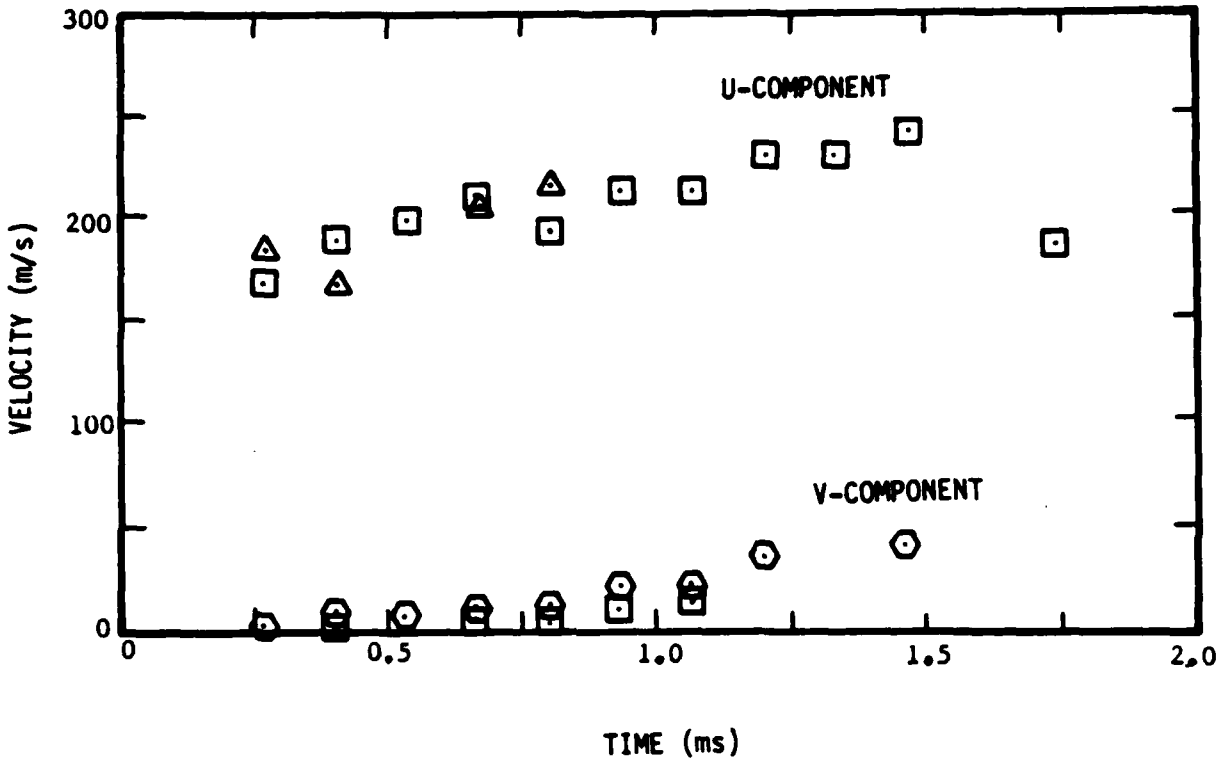

Figure 27. Particle Velocity Time History at TRW 4" Shock Tube, Y = 6 mm.

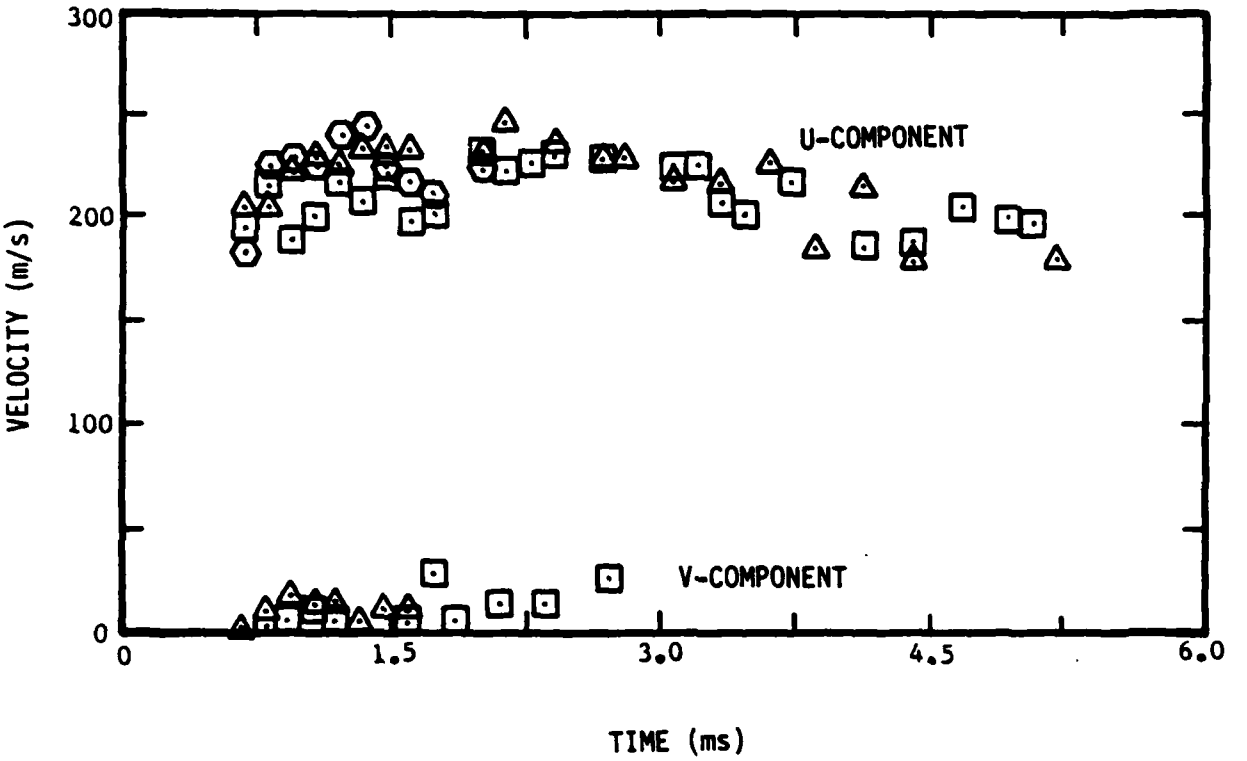

Figure 28. Particle Velocity Time History at TRW 4" Shock Tube, Y = 12 mm.

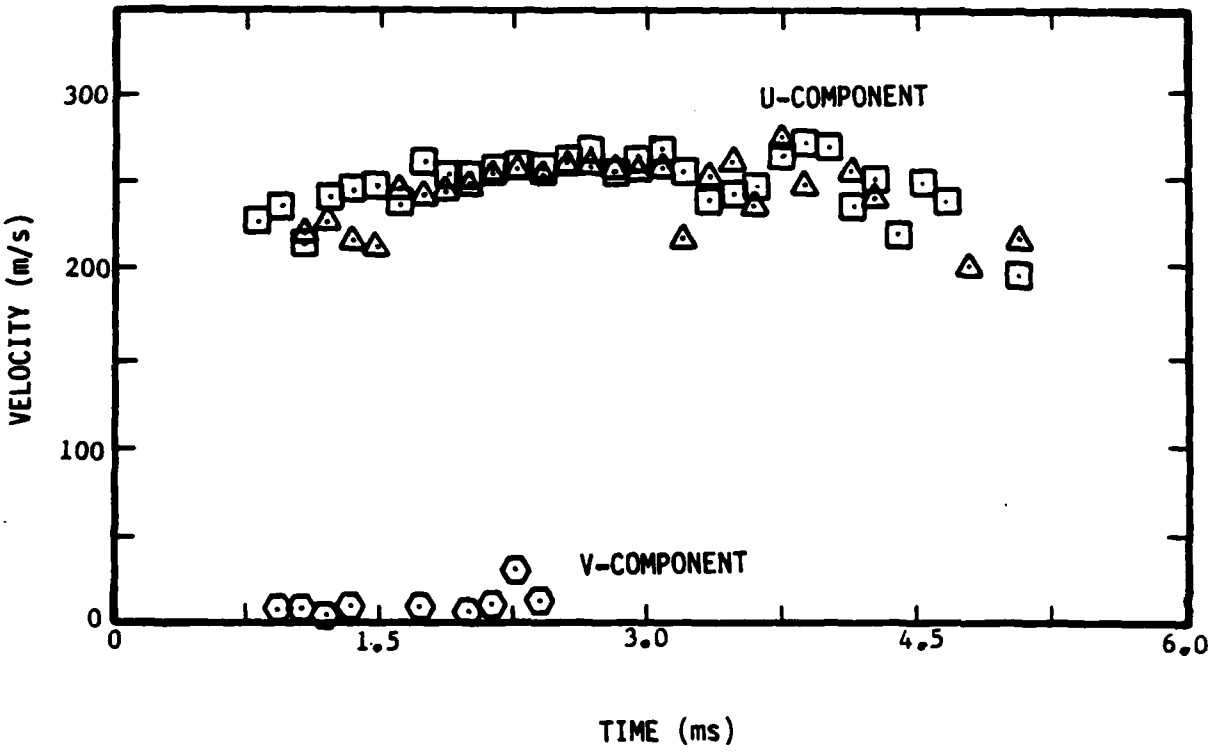

Figure 29. Particle Velocity Time History at TRW 4" Shock Tube, Y = 18 mm.

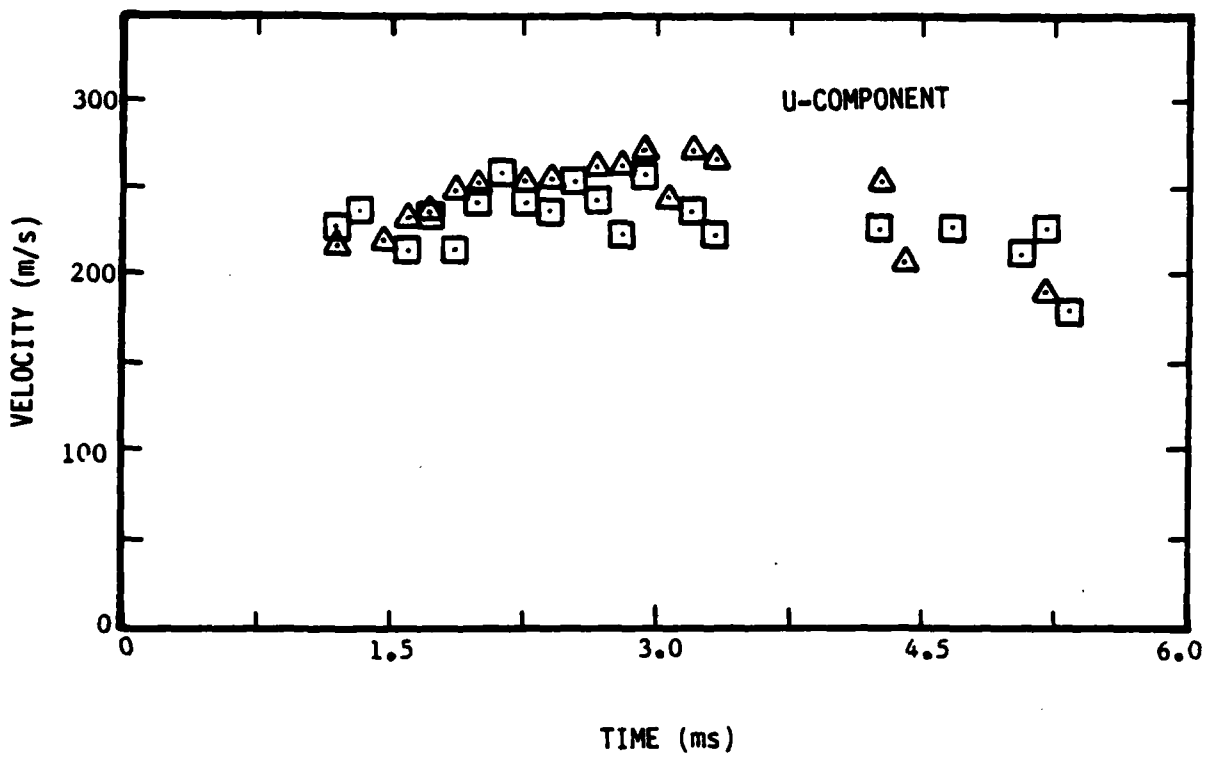

Figure 30. Particle Velocity Time History at TRW 4" Shock Tube, Y = 25 mm.

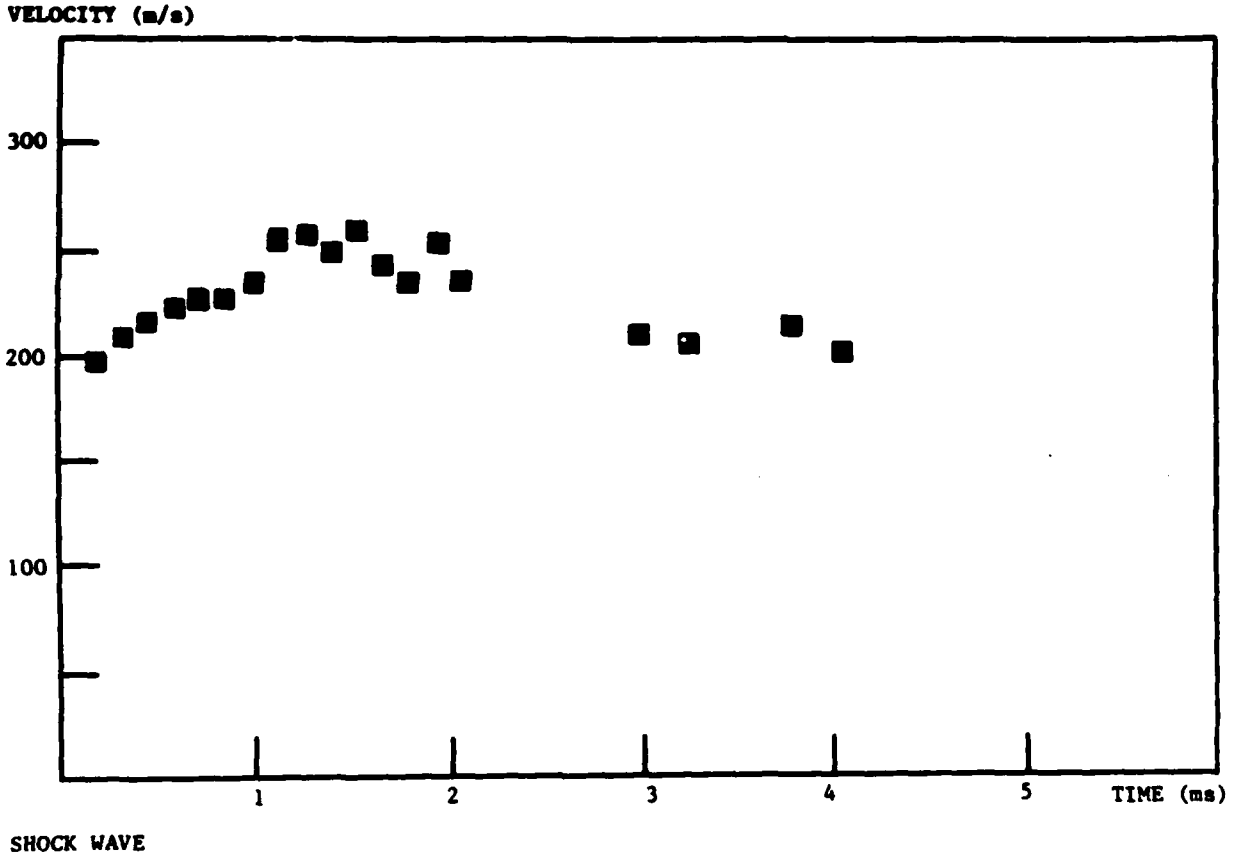

Figure 31. Streamwise Particle Velocity at TRW 4" Tube, Shock Wave, Y = 6 mm.

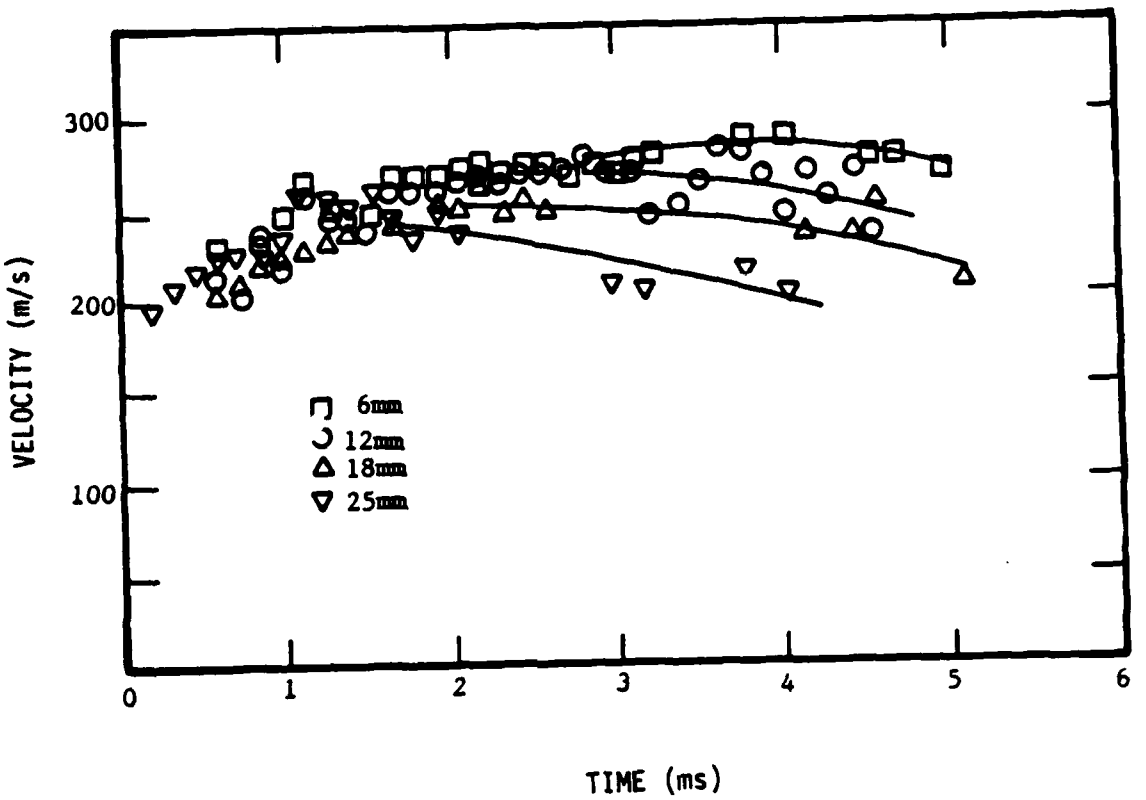

Figure 32. Streamwise Particle Velocity Component Behind the Shock Wave for All Heights.

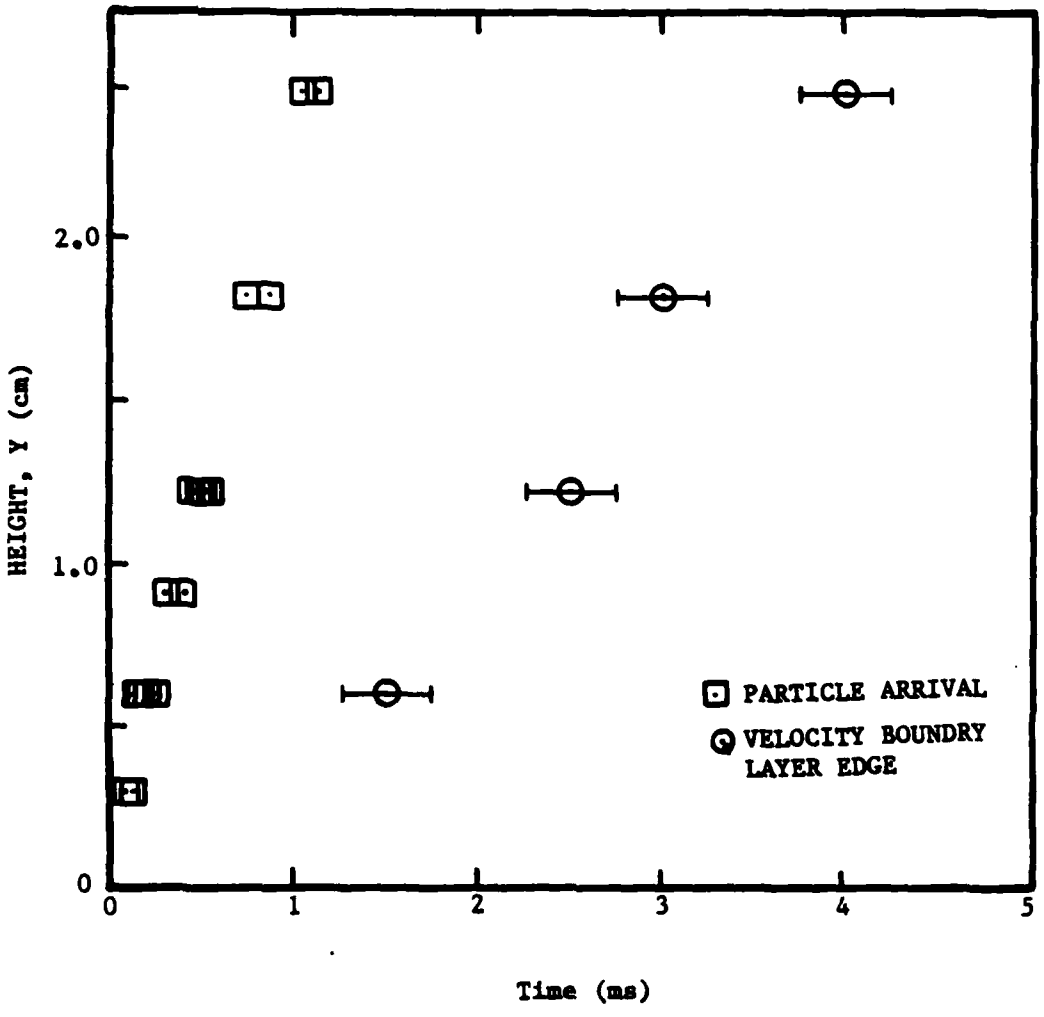

Figure 33. Dusty Flow Boundry Layer for TRW 4".

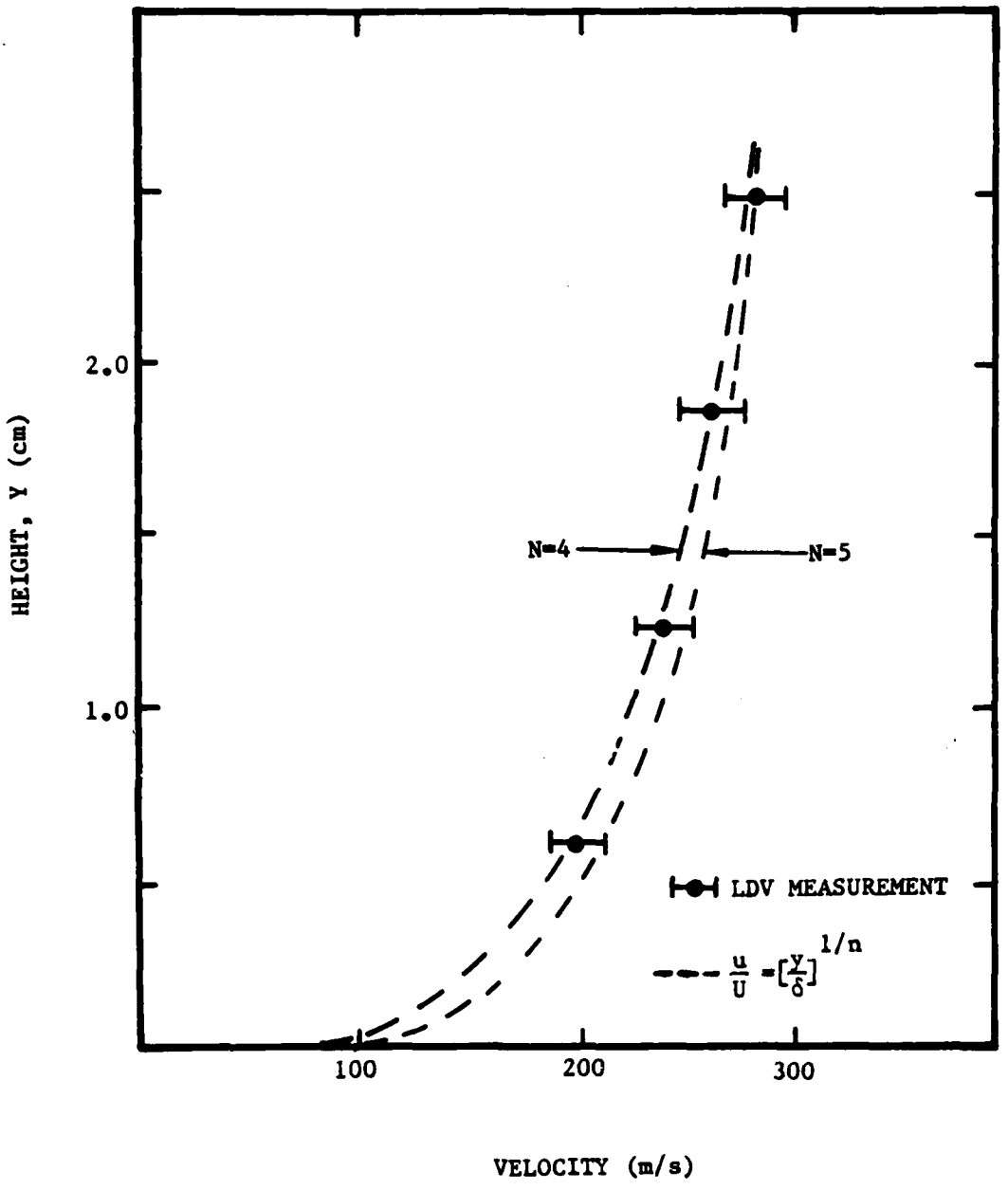

Figure 34. Particle Velocity Profile 4ms Behind the Shock Wave.

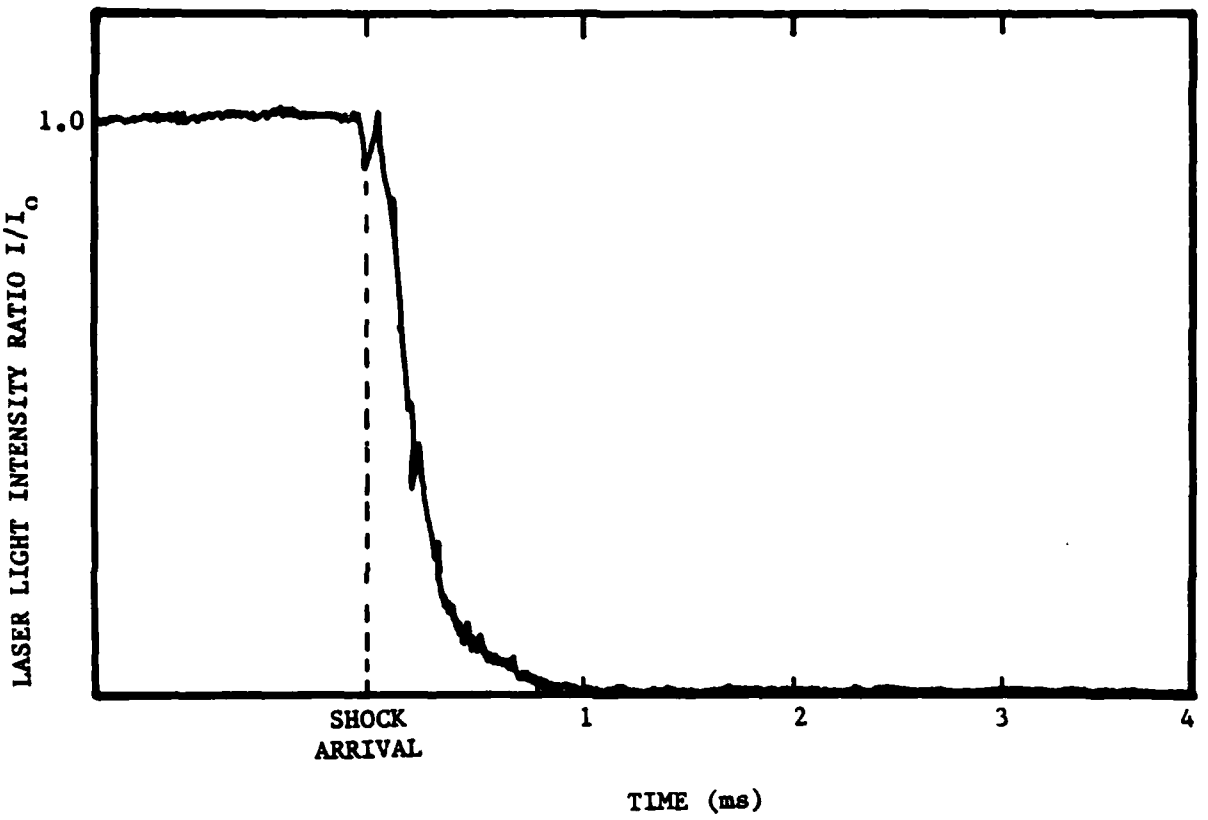

Figure 35. Laser Light Extinction, Y = 6 mm.

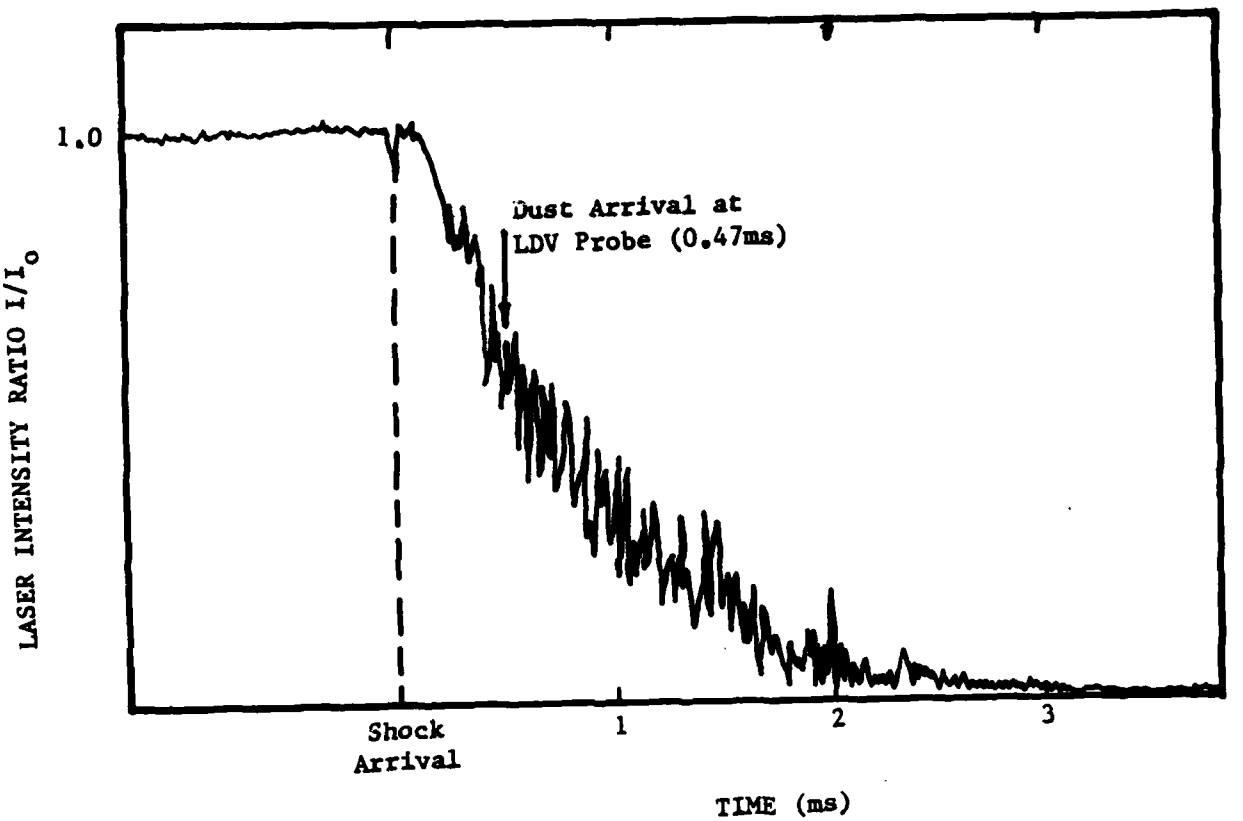

Figure 36. Laser Light Extinction, Y = 12 mm.

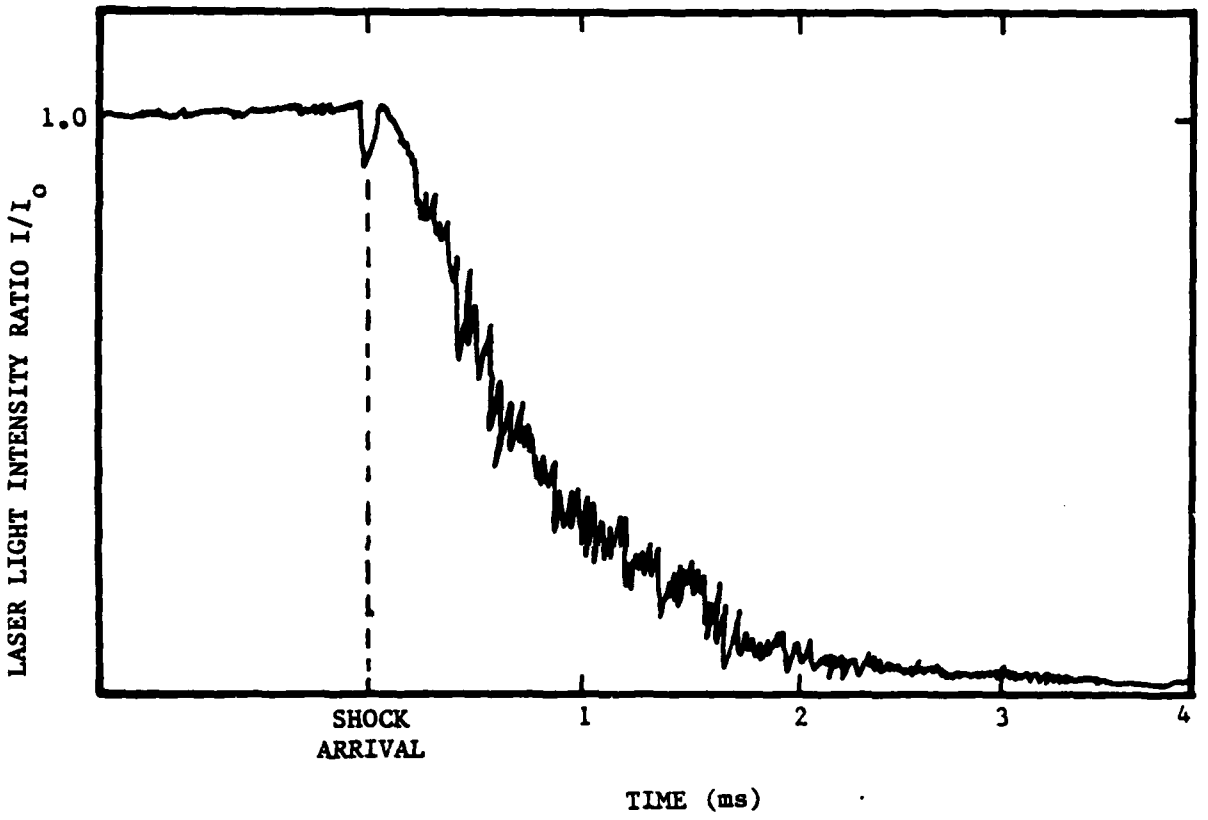

Figure 37. Laser Light Extinction, Y = 18 mm.

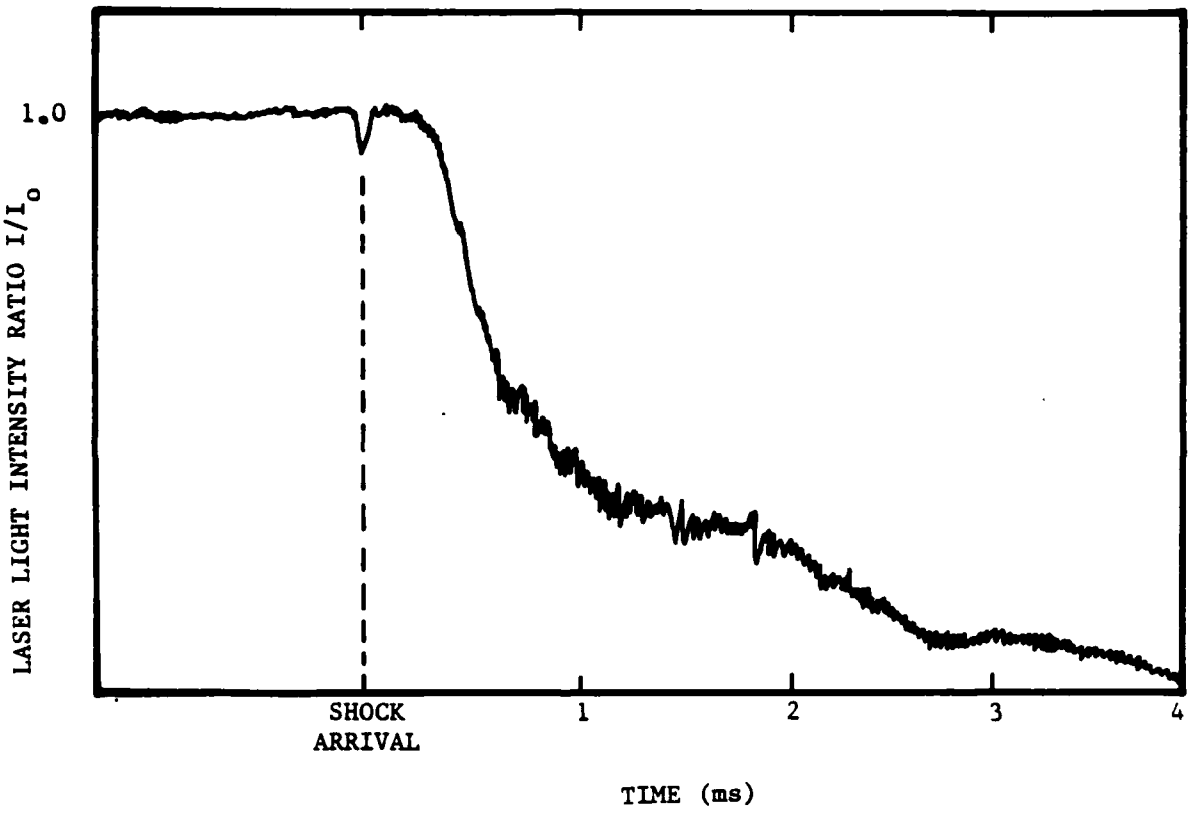

Figure 38. Laser Light Extinction, Y = 25 mm.

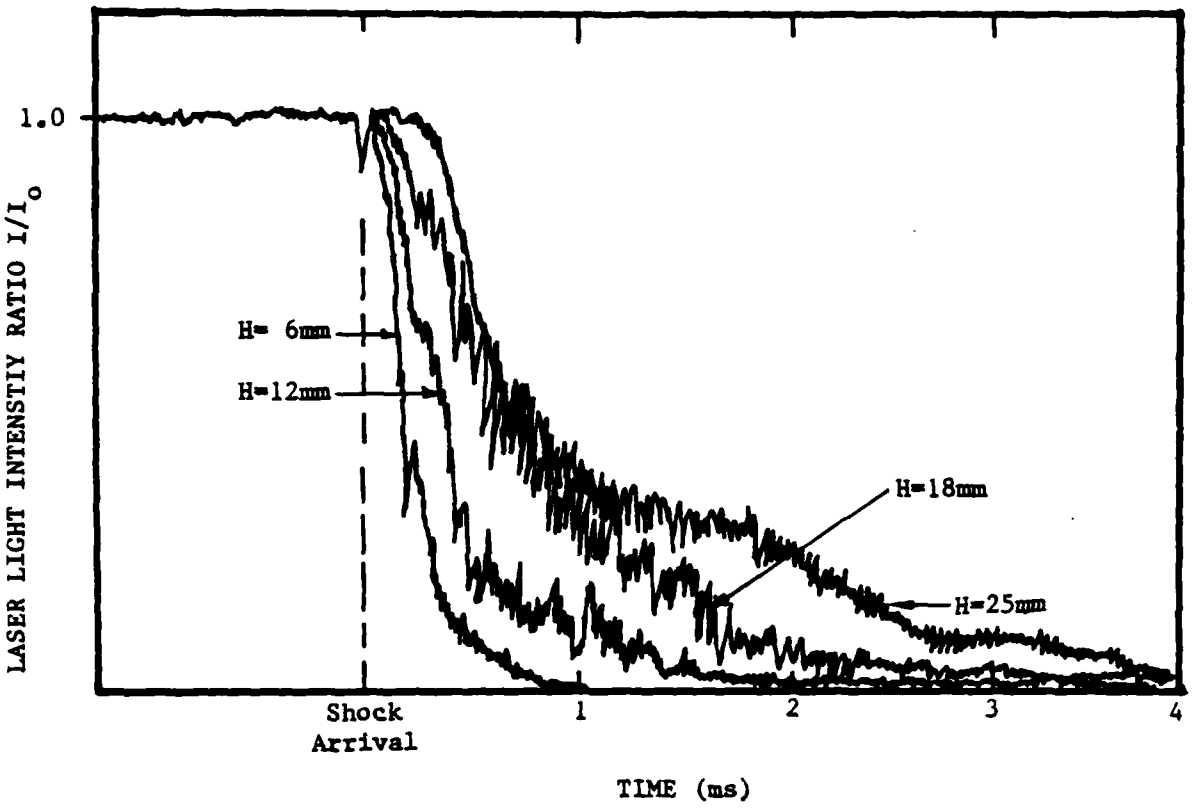

Figure 39. Laser Light Extinction Across the Shock Tube for All Heights.

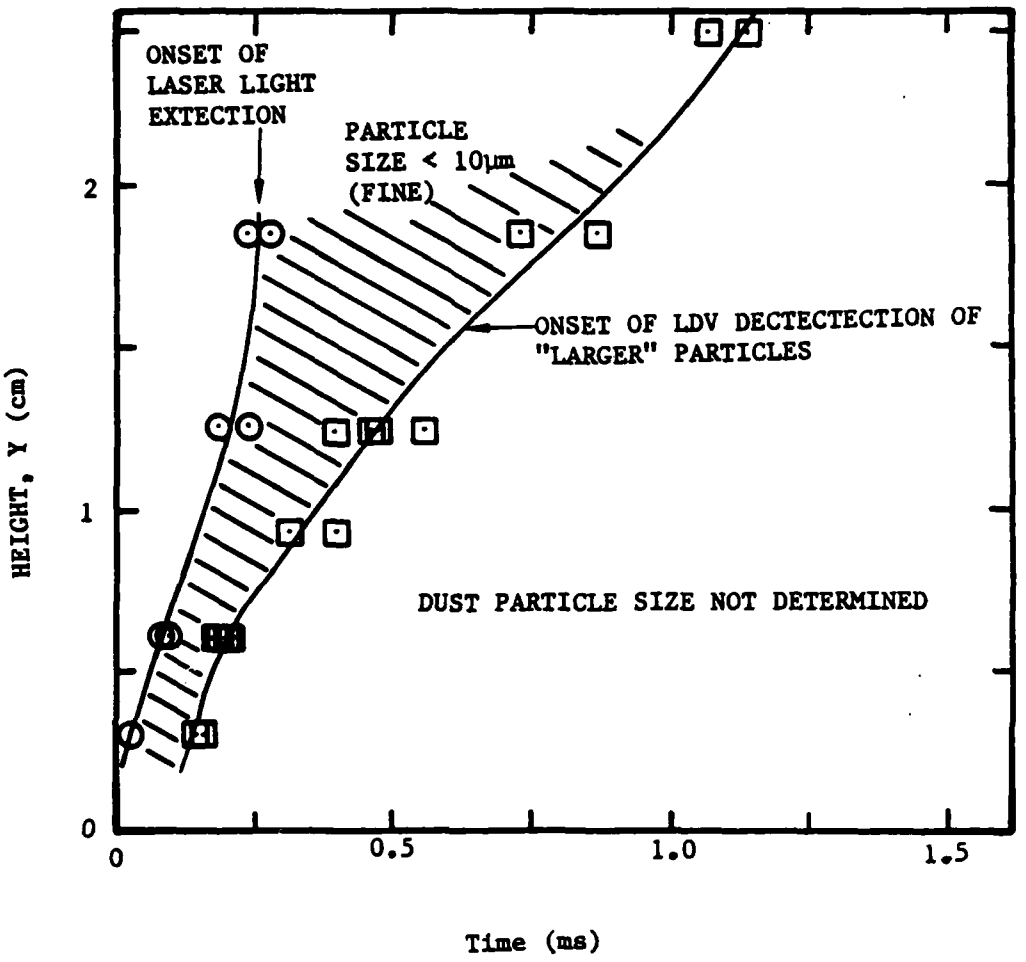

Figure 40. Dust Particle Size Group.

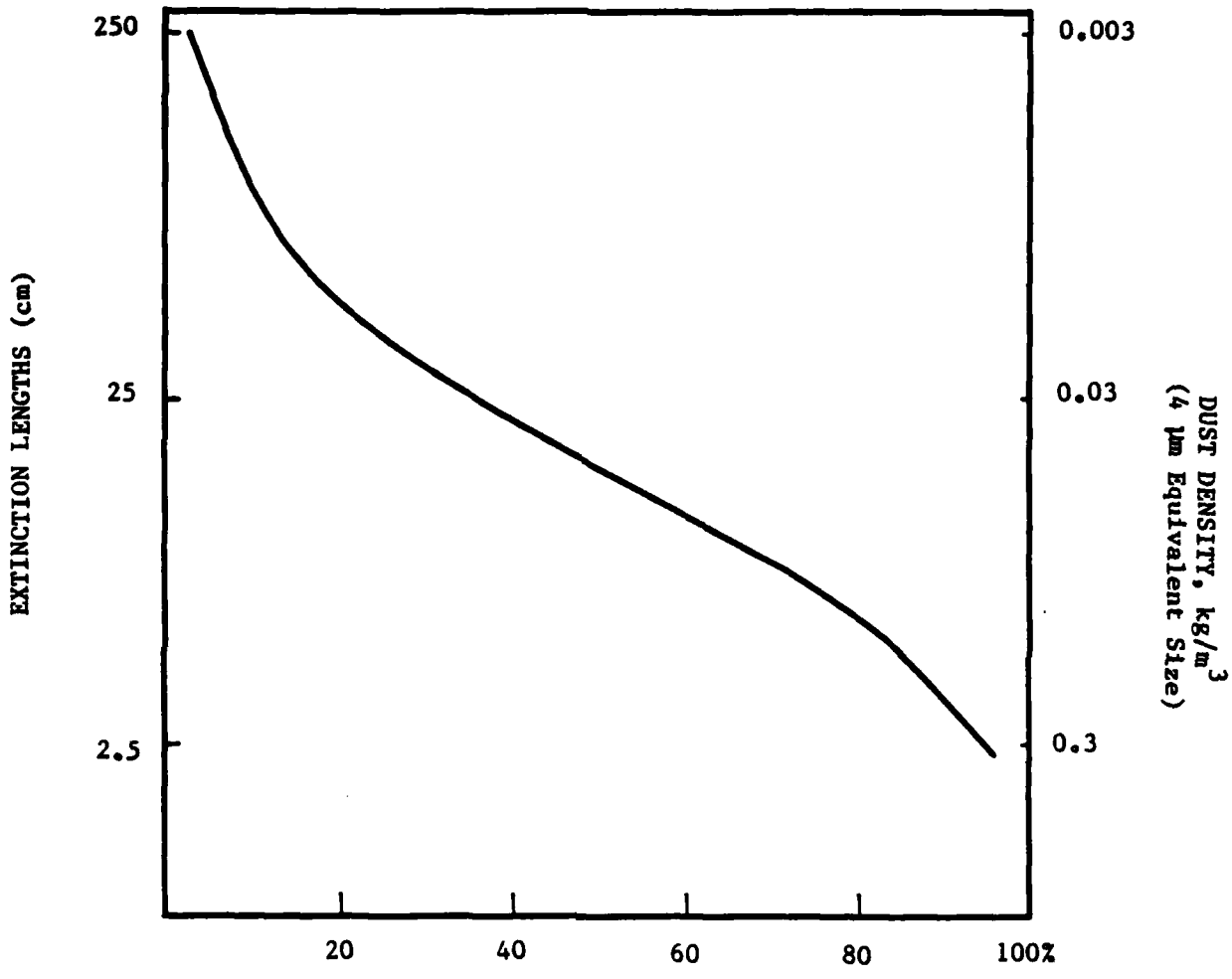

Figure 41. Laser Light Extinction Calibration Curve.

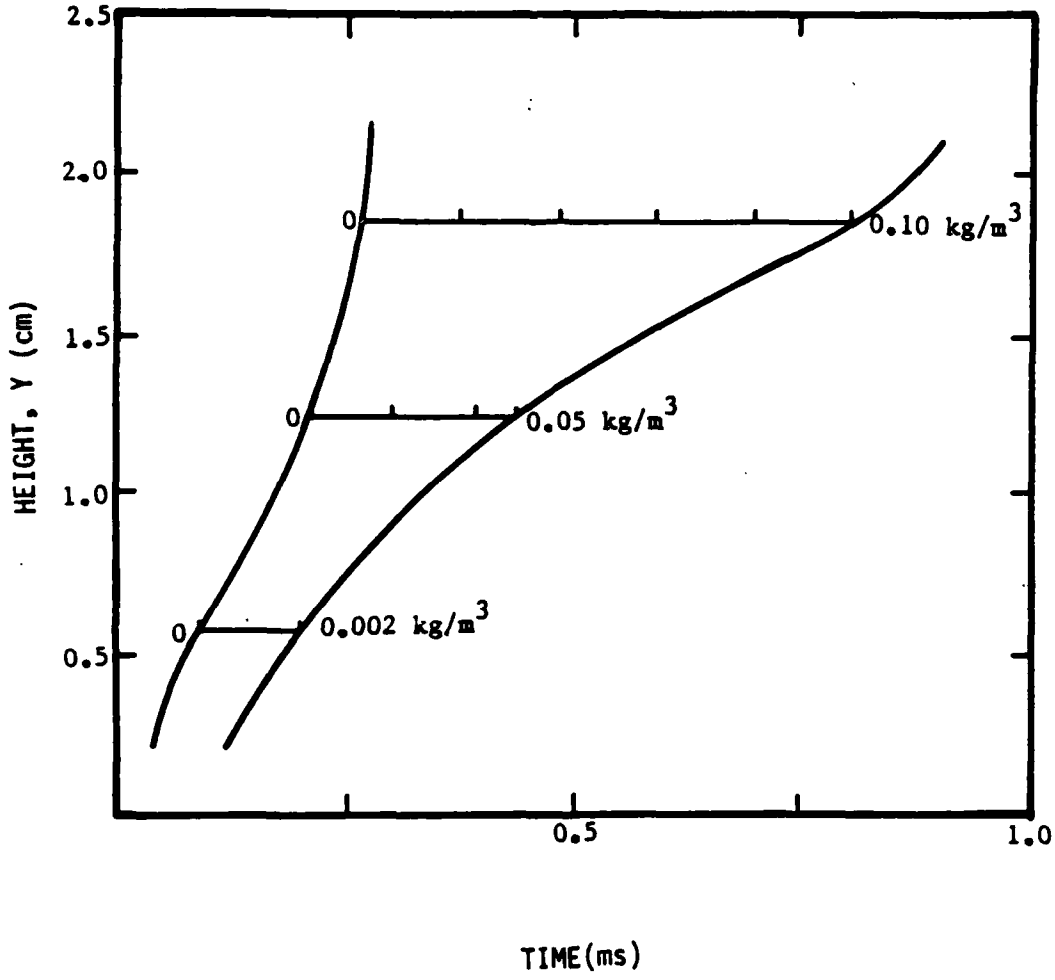

Figure 42. Dust Concentration.

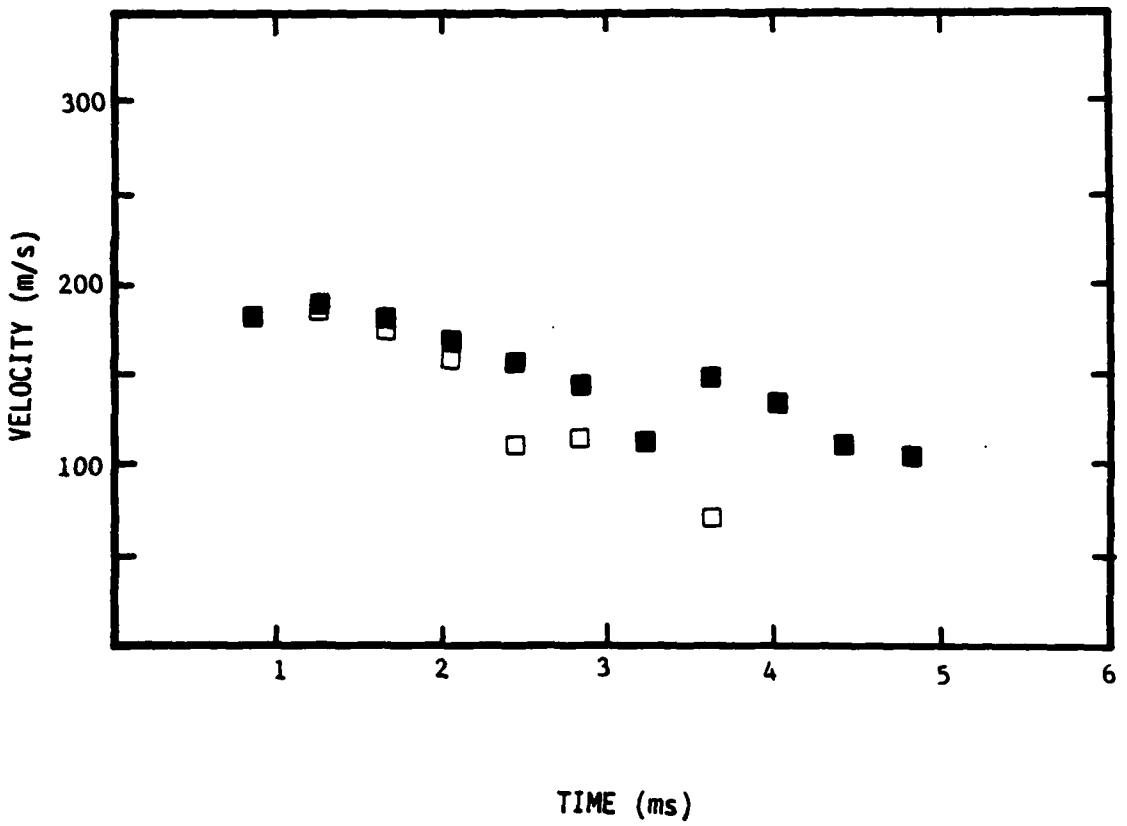

Figure 43. Particle Velocity Time History at CERF 6' Shock Tube, Y = 12 mm.

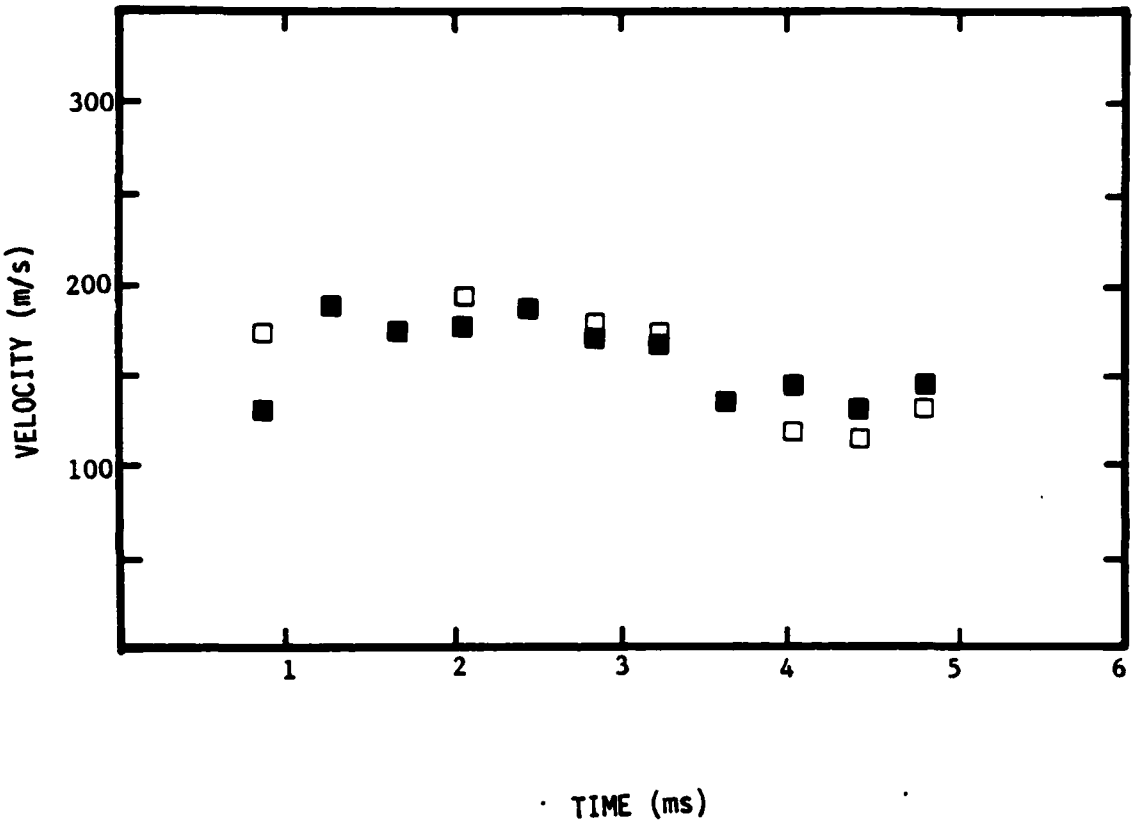

Figure 44. Particle Velocity Time History at CERF 6' Shock Tube, Y = 25 mm.

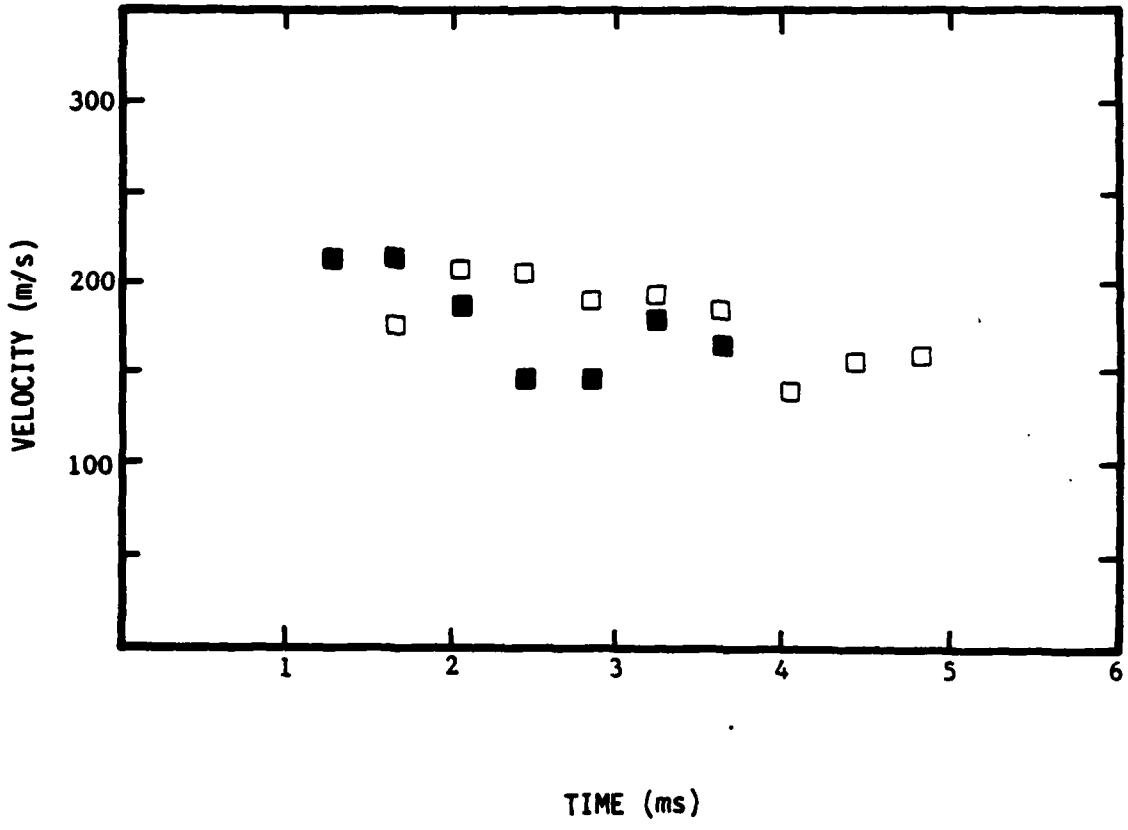

Figure 45. Particle Velocity Time History at CERF 6' Shock Tube, Y = 36 mm.

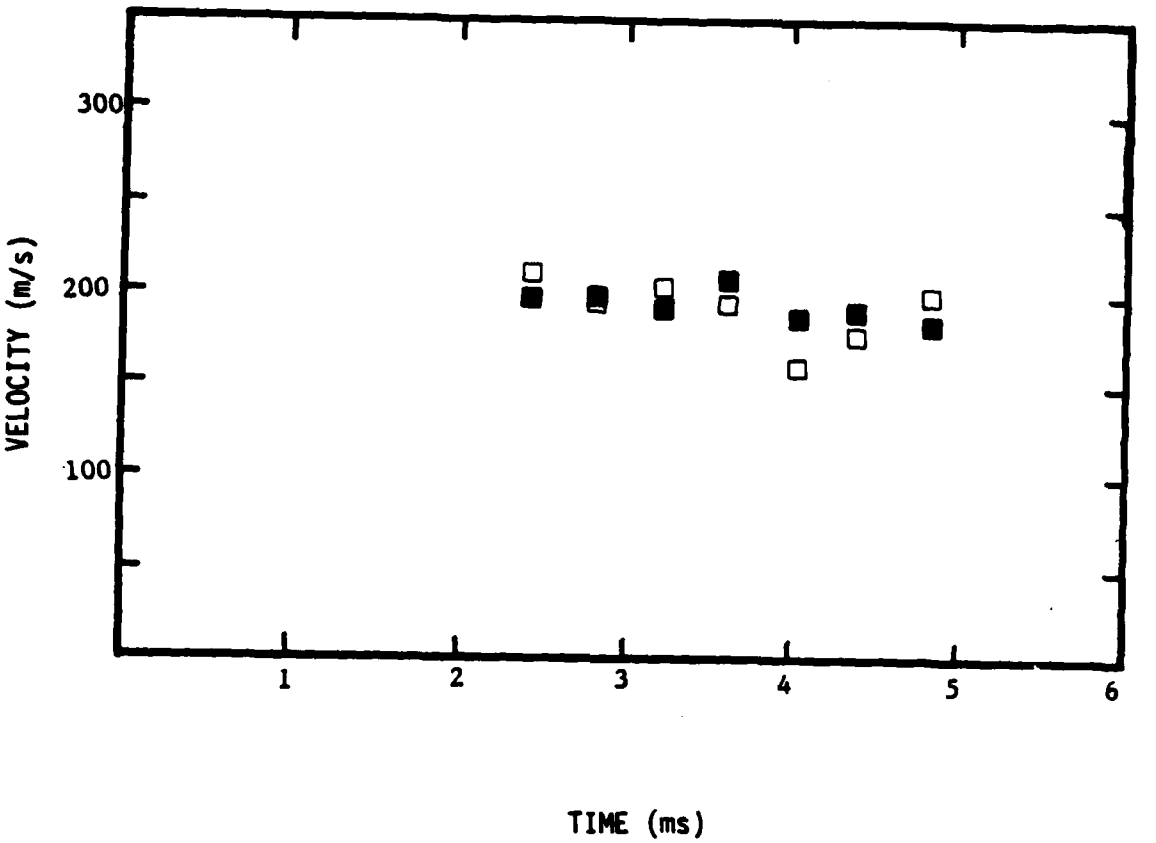

Figure 46. Particle Velocity Time History at CERF 6' Shock Tube, Y = 60 mm.

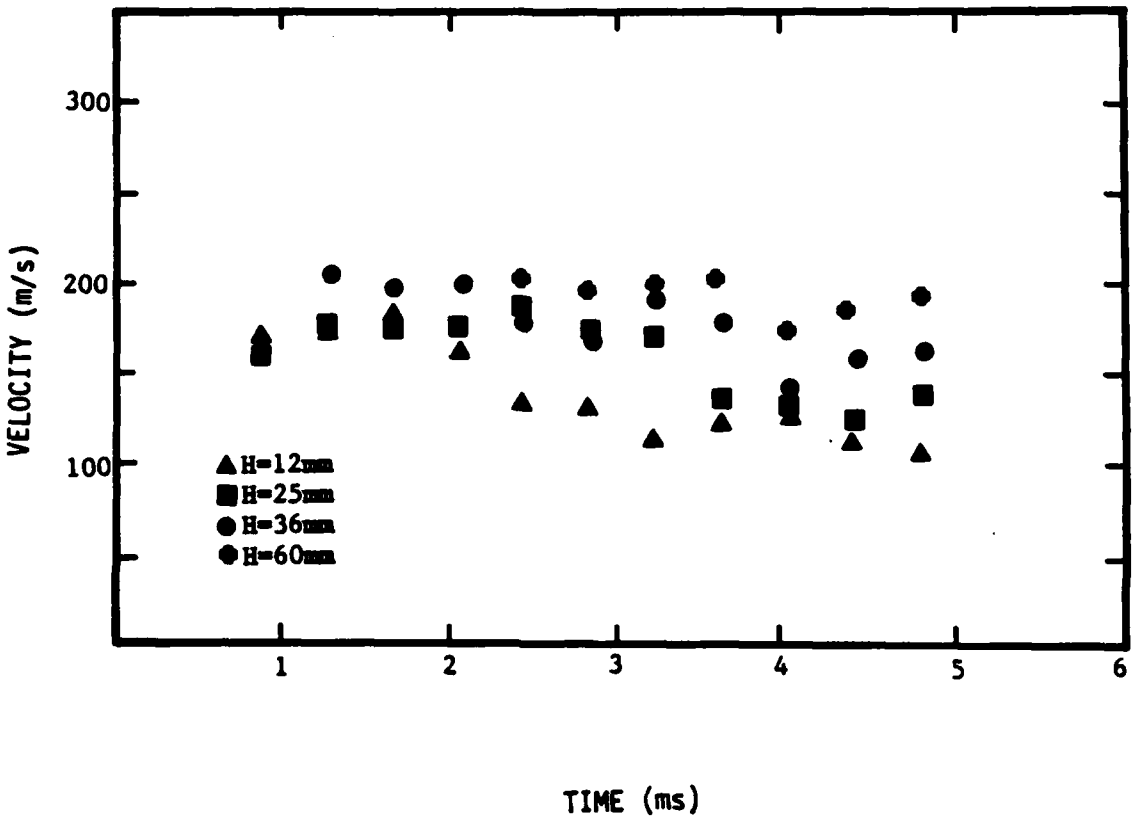

Figure 47. Particle Velocity Time History at CERF 6' Shock Tube, All Heights.

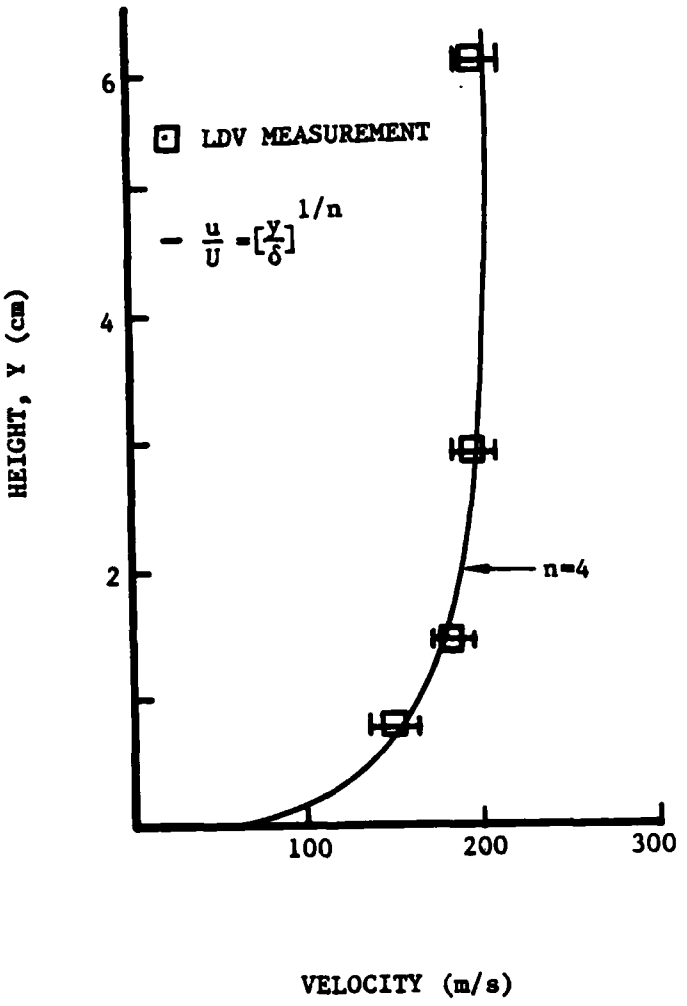

Figure 48. Velocity Profile at 2 ms Behind Shock Wave.

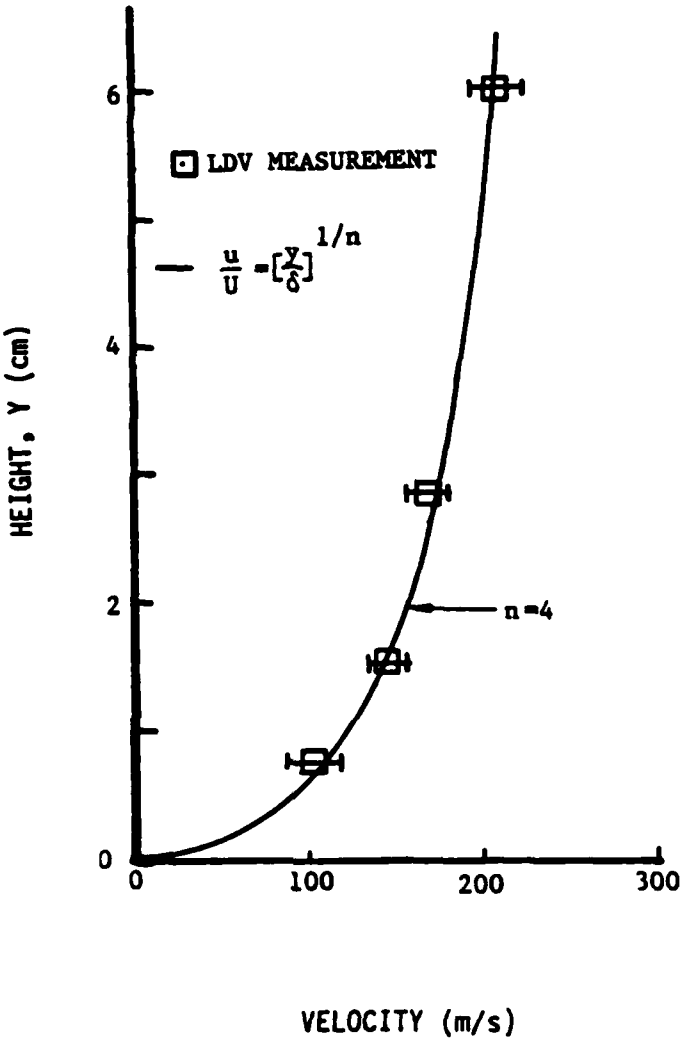

Figure 49. Velocity Profile at 4 mm Behind Shock Wave.

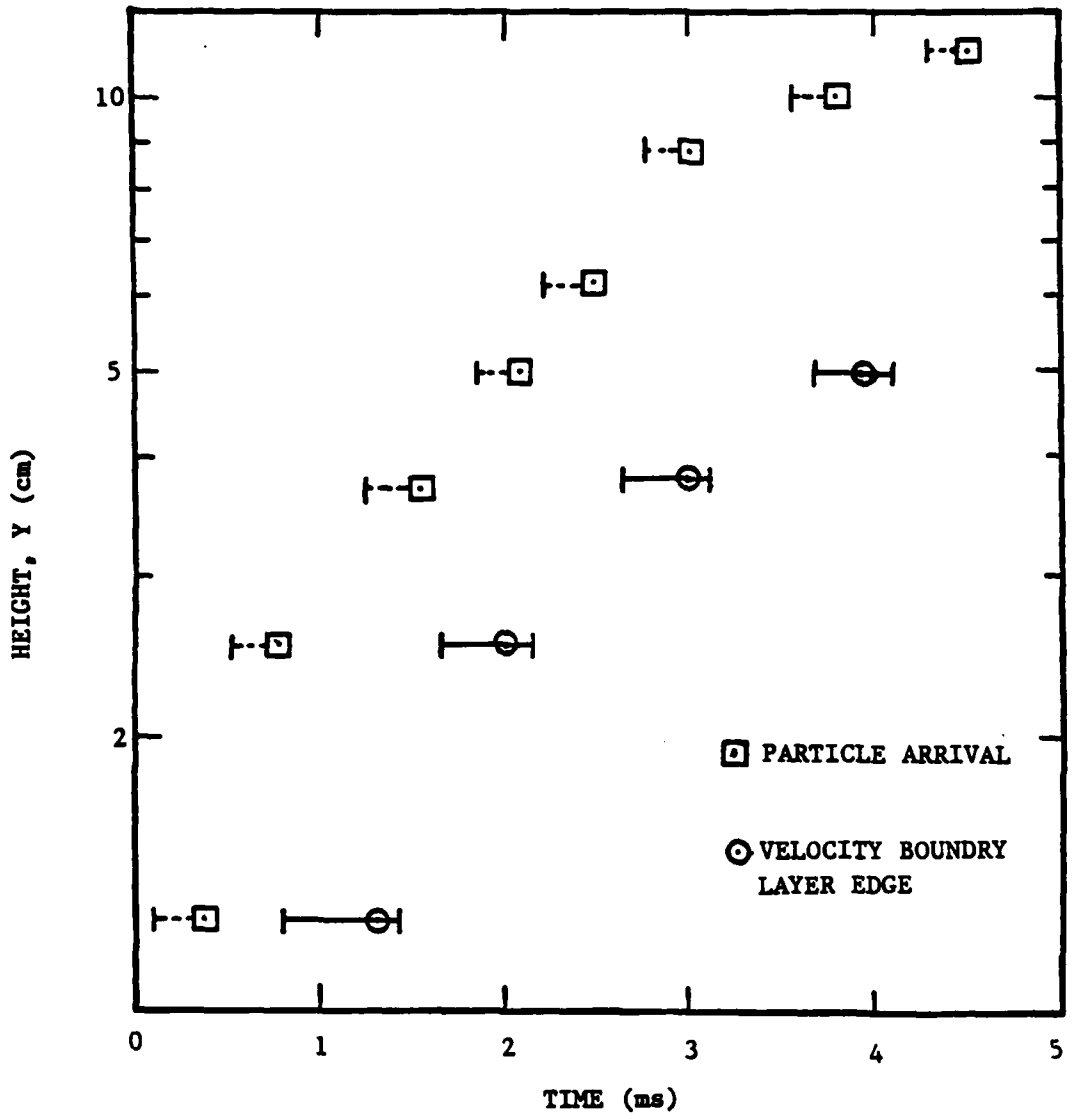

Figure 50. Dusty Flow Boundry Layer for CERF 6'.

DISTRIBUTION LIST

DEPARTMENT OF DEFENSE

AIR FORCE SOUTH
ATTN: U S DOCS OFFICER

ASST TO THE SECY OF DEF ATOMIC ENERGY
ATTN: EXECUTIVE ASSISTANT

DEFENSE INTELLIGENCE AGENCY
ATTN: DT-2
ATTN: RTS
ATTN: RTS-2B

DEFENSE NUCLEAR AGENCY
ATTN: SPAS
ATTN: STSP
4 CYS ATTN: STTI-CA

DEFENSE TECHNICAL INFORMATION CENTER
12 CYS ATTN: DD

FIELD COMMAND DNA DET 2
LAWRENCE LIVERMORE NATIONAL LAB
ATTN: FC-1

FIELD COMMAND DEFENSE NUCLEAR AGENCY
ATTN: FCPR
ATTN: FCT COL J MITCHELL
ATTN: FCTT W SUMMA
ATTN: FCTXE

JOINT CHIEFS OF STAFF
ATTN: J-5 NUC & CHEM DIV

JOINT STRAT TGT PLANNING STAFF
ATTN: JLK (ATTN: DNA REP)
ATTN: JLKS
ATTN: JPPFM
ATTN: JPTP

UNDER SECY OF DEF FOR RSCH & ENGRG
ATTN: STRAT & SPACE SYS (OS)
ATTN: STRAT & THR NUC FOR J THOMPSON
ATTN: STRAT & THEATER NUC FORCES

DEPARTMENT OF THE ARMY

DEP CH OF STAFF FOR OPS & PLANS
ATTN: DAMO-NCZ

HARRY DIAMOND LABORATORIES
ATTN: SLCHD-NW-RH

U S ARMY MATERIAL COMMAND
ATTN: AMCCN

U S ARMY MATERIAL TECHNOLOGY LABORATORY
ATTN: DRXMR-HH

U S ARMY STRATEGIC DEFENSE CMD
ATTN: DACS-BM TECHNOLOGY DIV

U S ARMY STRATEGIC DEFENSE COMMAND
ATTN: ATC-D (WATTS)
ATTN: ATC-R (ANDREWS)

DEPARTMENT OF THE NAVY

NAVAL RESEARCH LABORATORY
ATTN: CODE 2627 TECH LIB
ATTN: CODE 4040 D BOOK

NAVAL SEA SYSTEMS COMMAND
ATTN: SEA-0351

NAVAL SURFACE WEAPONS CENTER
ATTN: CODE K82
ATTN: CODE R44 H GLAZ

OFC OF THE DEPUTY CHIEF OF NAVAL OPS
ATTN: NOP 654 STRAT EVAL & ANAL BR

STRATEGIC SYSTEMS PROGRAMS (PM-1)
ATTN: SP-272

DEPARTMENT OF THE AIR FORCE

AIR FORCE SYSTEMS COMMAND
ATTN: DLW

AIR FORCE WEAPONS LABORATORY, AFSC
ATTN: NTED J RENICK
ATTN: NTED LT KITCH
ATTN: NTED R HENNY
ATTN: NTEDA
ATTN: NTES
ATTN: SUL

AIR FORCE WRIGHT AERONAUTICAL LAB
ATTN: FIBC
ATTN: FIMG

AIR FORCE WRIGHT AERONAUTICAL LAB
ATTN: AFWAL/MLP
ATTN: AFWAL/MLTM

DEPARTMENT OF THE AIR FORCE (CONTINUED)

AIR UNIVERSITY LIBRARY
ATTN: AUL-LSE

BALLISTIC MISSILE OFFICE/DAA
ATTN: CAPT T KING MGEN
ATTN: CC MAJ GEN CASEY
ATTN: ENSR

DEPUTY CHIEF OF STAFF/AF-RDQI
ATTN: AF/RDQI

DEPUTY CHIEF OF STAFF/AFRDS
ATTN: AFRDS SPACE SYS & C3 DIR

STRATEGIC AIR COMMAND/NRI-STINFO
ATTN: NRI/STINFO

STRATEGIC AIR COMMAND/XPQ
ATTN: XPQ

161 ARG ARIZONA ANG
ATTN: LTCOL SHERER

DEPARTMENT OF ENERGY

UNIVERSITY OF CALIFORNIA
LAWRENCE LIVERMORE NATIONAL LAB
ATTN: D BURTON
ATTN: L-10 J CAROTHERS
ATTN: L-122 G GOUDREAU
ATTN: L-122 S SACKETT
ATTN: L-203 T BUTKOVICH
ATTN: L-22 D CLARK
ATTN: L-8 P CHRZANOWSKI
ATTN: L-84 H KRUGER

LOS ALAMOS NATIONAL LABORATORY
ATTN: A112 MS R SELDEN
ATTN: M T SANDFORD
ATTN: R WHITAKER

SANDIA NATIONAL LABORATORIES
ATTN: D J RIGALI
ATTN: ORG 7112 A CHABAI
ATTN: R G CLEM

OTHER GOVERNMENT

CENTRAL INTELLIGENCE AGENCY
ATTN: OSWR/NED

DEPARTMENT OF THE INTERIOR
ATTN: D RODDY

DEPARTMENT OF DEFENSE CONTRACTORS

ACUREX CORP
ATTN: C WOLF

AEROSPACE CORP
ATTN: H MIRELS

APPLIED RESEARCH ASSOCIATES, INC
ATTN: N HIGGINS

APPLIED RESEARCH ASSOCIATES, INC
ATTN: S BLOUIN

APPLIED RESEARCH ASSOCIATES, INC
ATTN: D PIEPENBURG

BELL AEROSPACE TEXTRON
ATTN: C TILYOU

CALIFORNIA RESEARCH & TECHNOLOGY, INC
ATTN: K KREYENHAGEN
ATTN: M ROSENBLATT

CALIFORNIA RESEARCH & TECHNOLOGY, INC
ATTN: F SAUER

H-TECH LABS, INC
ATTN: B HARTENBAUM

INFORMATION SCIENCE, INC
ATTN: W DUDZIAK

KAMAN SCIENCES CORP
ATTN: L MENTE
ATTN: R RUETENIK
ATTN: W LEE

KAMAN TEMPO
ATTN: DASIAC

KAMAN TEMPO
ATTN: DASIAC

MAXWELL LABORATORIES, INC
ATTN: J MURPHY

MERRITT CASES, INC
ATTN: J MERRITT

NEW MEXICO ENGINEERING RESEARCH INSTITUTE
ATTN: G LEIGH

PACIFIC-SIERRA RESEARCH CORP
ATTN: H BRODE, CHAIRMAN SAGE

R & D ASSOCIATES
ATTN: A KUHL
ATTN: C K B LEE
ATTN: J LEWIS
ATTN: P RAUSCH

DEPT OF DEFENSE CONTRACTORS (CONTINUED)

R & D ASSOCIATES
ATTN: P MOSTELLER

S-CUBED
ATTN: A WILSON

S-CUBED
ATTN: C NEEDHAM

SCIENCE APPLICATIONS INTL CORP
ATTN: H WILSON

SCIENCE APPLICATIONS INTL CORP
ATTN: J COCKAYNE
ATTN: W LAYSON

SCIENCE APPLICATIONS INTL CORP
ATTN: A MARTELLUCCI

SCIENCE APPLICATIONS INTL CORP
ATTN: G BINNINGER

SPECTRON DEVELOPMENT LABS, INC
2 CYS ATTN: M DARIUSH

TRW ELECTRONICS & DEFENSE SECTOR
ATTN: G HULCHER
ATTN: P DAI

WEIDLINGER ASSOC, CONSULTING ENGRG
ATTN: P WEIDLINGER

END

DTIC

10-86